National Library of Canada
Bibliothèque nationale du Canada

Canadian Theses Service
Service des thèses canadiennes

Ottawa, Canada
K1A 0N4

NOTICE

The quality of this microform is heavily dependent upon the quality of the original thesis submitted for microfilming. Every effort has been made to ensure the highest quality of reproduction possible.

If pages are missing, contact the university which granted the degree.

Some pages may have indistinct print especially if the original pages were typed with a poor typewriter ribbon or if the university sent us an inferior photocopy.

Reproduction in full or in part of this microform is governed by the Canadian Copyright Act, R.S.C. 1970, c. C-30, and subsequent amendments.

AVIS

La qualité de cette microforme dépend grandement de la qualité de la thèse soumise au microfilmage. Nous avons tout fait pour assurer une qualité supérieure de reproduction.

S'il manque des pages, veuillez communiquer avec l'université qui a conféré le grade.

La qualité d'impression de certaines pages peut laisser à désirer, surtout si les pages originales ont été dactylographiées à l'aide d'un ruban usé ou si l'université nous a fait parvenir une photocopie de qualité inférieure.

La reproduction, même partielle, de cette microforme est soumise à la Loi canadienne sur le droit d'auteur, SRC 1970, c. C-30, et ses amendements subséquents.

NL-339 (r. 88/04) c

Canada

THE UNIVERSITY OF ALBERTA

A RADIO FREQUENCY CARBON DIOXIDE SLAB LASER

BY

ALAN W. MITCHELL

A THESIS

SUBMITTED TO THE FACULTY OF GRADUATE STUDIES AND RESEARCH

IN PARTIAL FULFILIMENT OF THE REQUIREMENTS FOR THE DEGREE

OF MASTER OF SCIENCE

DEPARTMENT OF ELECTRICAL ENGINEERING

EDMONTON, ALBERTA

SPRING, 1990

National Library of Canada
Bibliothèque nationale du Canada

Canadian Theses Service
Service des thèses canadiennes

Ottawa, Canada
K1A 0N4

NOTICE

The quality of this microform is heavily dependent upon the quality of the original thesis submitted for microfilming. Every effort has been made to ensure the highest quality of reproduction possible.

If pages are missing, contact the university which granted the degree.

Some pages may have indistinct print especially if the original pages were typed with a poor typewriter ribbon or if the university sent us an inferior photocopy.

Reproduction in full or in part of this microform is governed by the Canadian Copyright Act, R.S.C. 1970, c. C-30, and subsequent amendments.

AVIS

La qualité de cette microforme dépend grandement de la qualité de la thèse soumise au microfilmage. Nous avons tout fait pour assurer une qualité supérieure de reproduction.

S'il manque des pages, veuillez communiquer avec l'université qui a conféré le grade.

La qualité d'impression de certaines pages peut laisser à désirer, surtout si les pages originales ont été dactylographiées à l'aide d'un ruban usé ou si l'université nous a fait parvenir une photocopie de qualité inférieure.

La reproduction, même partielle, de cette microforme est soumise à la Loi canadienne sur le droit d'auteur, SRC 1970, c. C-30, et ses amendements subséquents.

ISBN 0-315-60298-8

NL-339 (r. 88/04) c

Canada

THE UNIVERSITY OF ALBERTA

RELEASE FORM

NAME OF AUTHOR: Alan William Mitchell

TITLE OF THESIS: A Radio Frequency Carbon Dioxide Slab Laser

DEGREE: Master of Science

YEAR THIS DEGREE GRANTED: 1990

Permission is hereby granted to THE UNIVERSITY OF ALBERTA LIBRARY to reproduce single copies of this thesis and to lend or sell such copies for private, scholarly or scientific research purposes only.

The author reserves other publication rights, and neither the thesis nor extensive extracts from it may be printed or otherwise reproduced without the author's written permission.

(SIGNED) .....

PERMANENT ADDRESS:

10676 - 59 St.

Edmonton, Alberta

T6E 2K7

DATED Apr. 20 1990

THE UNIVERSITY OF ALBERTA

FACULTY OF GRADUATE STUDIES AND RESEARCH

The undersigned certify that they have read, and recommend to the Faculty of Graduate Studies and Research for acceptance, a thesis entitled A Radio Frequency Carbon Dioxide Slab Laser submitted by Alan William Mitchell in partial fulfillment of the requirements for the degree of Master of Science.

.....

Dr. J. Tulip, Supervisor

.....

Dr. H. J. J. Seguin

.....

Dr. D. N. Dederich

Date April 11/90

To My Parents

Abstract

Radio frequency (RF) excited carbon dioxide waveguide lasers have become a staple in the low power, 1 to 30 watt, area. Good stability, long lifetimes, and ease of use have been contributing factors of this design. To attain power levels in excess of 100 watts, new approaches to discharge scaling are needed. Area scaling has been attempted to overcome the power per unit length limitations of square bore RF waveguide lasers.

Lasers of cross–sectional dimensions of 2.25 mm by 10, 30, and 50 mm have been constructed, with active region lengths of 30 and 60 cm. Gas optimization in both pressure and mixture was carried out for these lasers. A gas mixture of 3:1:1 ($He:CO_2:N_2$) was found to produce the best efficiencies at kilowatt discharge power loadings. Efficiencies of 10% to 12% are reported at laser power outputs of 99 watts.

Unstable resonators were used for optimal power extraction and good beam properties from the slab discharge. Lower power extraction efficiencies than conventional stable resonators were noted. Beam profile analysis was done, finding that standard geometrical design techniques do not hold for small output coupling resonators (5% to 10%).

Preface

Throughout this work, the term slab laser will be used. This term is used since the electrode plates bound the discharge into a slab. Use of the term "slab" will always refer to the slab laser. The notation used to track the various revisions of these lasers will be referred to, for example, as 1/30 cm. This represents the width/length of the discharge and waveguide assembly. It is used consistently as it forms a unique tag with which to refer to a given laser variation.

Acknowledgement

Without Dr. John Tulip none of the work for this thesis would have been completed, nor even attempted. I am thankful to have had the opportunity to examine this area with his guidance.

Thanks must be given to H. Gans, and G. Fij, and the rest of the machine shop for their work on the various slab laser revisions. It was through their skill that this was possible.

A special mention must be given to K. Westra, B. McArthur, B. Bathgate, and M. Paulson for their initial work on the slab laser. Many thanks to M. Paulson for the many discussions concerning lasers and RF networks. I would like to thank G. McKinnon for the use of AMC facilities which greatly helped in the production of my thesis.

In every acknowledgment, someone is forgotten who was instrumental in helping to complete the work. I hope that any omissions will be forgiven and my thanks taken for all everyone has done.

Table of Contents

Chapter 1: Introduction to the Slab Laser 1

Chapter 2: Slab Laser Design 9
- 2.1 Waveguide Design 9
- 2.2 Vacuum Enclosure 15
- 2.3 Resonator Design 19
- 2.4 Electrical System 28

Chapter 3: The 3/30 Slab Laser and Optimization 33
- 3.1 Experimental Test Bench 33
- 3.2 Parameter Study and Optimization 36
- 3.3 Thermal Measurements 52
- 3.4 Optical Measurements 53
- 3.5 Power Scaling and the 1/30 Slab Laser 58
- 3.6 Conclusion 62

Chapter 4: 5/30 and 3/60 Slab Laser Optimization 63
- 4.1 5/30 Slab Laser 63
- 4.2 3/60 Slab Laser Design 69
- 4.3 Matching Networks 74
- 4.4 3/60 Experimental Results 76
- 4.5 Conclusion 97

Chapter 5: Conclusion 98

List of Tables

Chapter 1: Introduction to the Slab Laser 1

Chapter 2: Slab Laser Design 9

2.1 Propagation Loss Coefficients 12

2.2 Thermal Constants of Waveguide Materials 14

2.3 Advantages of The Confocal Unstable Resonator 20

2.4 Confocal Unstable Resonator Parameters 26

Chapter 3: The 3/30 Slab Laser and Optimization 33

Chapter 4: 5/30 and 3/60 Slab Laser Optimization 63

4.1 Optical Resonator Geometrical Coupling Experiment 82

4.2 Operating Temperatures for 3/60 Slab Laser 95

Chapter 5: Conclusion 98

List Of Figures

Chapter 1: Introduction to the Slab Laser 1

Chapter 2: Slab Laser Design 9

2.1 Cross-Section of Rectangular Waveguide 11
2.2 Cross-Section of Slab Waveguide 11
2.3 Slab Laser Cross-Section 16
2.4 Cooling Channel Plate Cross-Section 17
2.5 Slab End Cross-Section 17
2.6 Optical Resonator Stability Diagram 22
2.7 Confocal Unstable Resonator 23
2.8 Off Axis Confocal Resonator 23
2.9 Experimental Electrical Network 29
2.10 Voltage Balancing Inductors 29

Chapter 3: The 3/30 Slab Laser and Optimization 33

3.1 Picture: Slab Laser Vacuum Housing 34
3.2 Picture: Vacuum System and RF Power Supply 35
3.3 Vacuum and Cooling Systems Piping Diagram 37
3.4 Laser Power Response of 3:1:1 Premix 40
3.5 Laser Power Response of 4:1:1 Pressure 41
3.6 Laser Power Response of 6:1:1 Pressure 42
3.7 Laser Power Response of 8:1:1 Pressure 43
3.8 Effect of Discharge Power on Laser Output, 3:1:1 44
3.9 Effect of Discharge Power on Laser Output, 4:1:1 45
3.10 Mixture Performance for 300 Watts Discharge Power 47
3.11 Mixture Performance for 400 Watts Discharge Power 48
3.12 Mixture Performance for 500 Watts Discharge Power 49
3.13 E/P for 3:1:1 on the 3/30 Slab 51
3.14 Experimental Beam Analysis Setup 55
3.15 Picture: Unstable Mode, Near Field of 3/30 Laser 57

3.16 Ficture: Far field of 3/30 Slab Laser 57
3.17 Power per Unit Width Comparison of 1/30 and 3/30 Lasers 60
3.18 Comparison of 1/30 and 3/30 Lasers 61

Chapter 4: 5/30 and 3/60 Slab Laser Optimization 63
4.1 Comparison of 3 cm and 5 cm Laser Power 65
4.2 Effect of Gas Pressure on 5/30 Laser Power: Low Pressure 66
4.3 Effect of Gas Pressure on 5/30 Laser Power: High Pressure 67
4.4 5/30 cm Laser Power and Efficiency 68
4.5 3/60 Slab Laser Cross–Section 71
4.6 3/60 Mirror Mount: Top View Cross–section 71
4.7 Matching Networks 75
4.8 Maximum Laser Power Produced for Gas Pressure 78
4.9 "Plexiglass" Mode Profile Experiment 80
4.10 Picture: 3/60 Slab Laser and Experiment Area 81
4.11 Picture: 5% Coupling Near Field, Side View 84
4.12 Picture: 5% Coupling Near Field, Top View 84
4.13 Picture: 5% Coupling Near Field, End View 85
4.14 Picture: 5% Coupling Far Field, Top View 85
4.15 Picture: ENAL Near Field, Side View 86
4.16 Picture: ENAL Near Field, Top View 86
4.17 Picture: ENAL Near Field, End View 87
4.18 Picture: ENAL Far Field, Top View 87
4.19 3/60 Laser: Using Flat Aluminum Mirrors 89
4.20 3/60 Laser Power and Efficiency at 40 torr 90
4.21 3/60 Laser Power and Efficiency at 45 torr 91
4.22 3/60 Laser Power and Efficiency at 50 torr 92
4.23 Picture: Vacuum System for Sealed Off Experiments 93

Chapter 5: Conclusion 98

List of Symbols

RF	Radio Frequency
E/P	Electric Field to Pressure Ratio
DC	Direct Current
α	Per Metre Loss Coefficient
n	Mode Number
ν	Complex Refractive Index
k	Wave Number
n_i	Refractive Index
K_i	Extinction Coefficient
EH	Electric Hybrid Mode
λ	Wave Length
g_i	Resonator Stability Parameter
R_i	Mirror Radius
δ	Geometric Resonator Coupling
A_{00}	Fundamental Waveguide Mode Coupling Fraction
ω_0	Gaussian Beam Waist
E/N	Electric Field to Atom Number Ratio
R_d	Discharge Resistance
m	Electron Mass
e	Electron Charge
d	Electrode Separation
ν	Electron Collision Frequency
n	Electron Density
F_0	Laser Resonant Frequency
L_b	Voltage Balancing Inductance
L_r	Resonant Inductance
C_l	Electrode Capacitance

Chapter 1: Introduction to the Slab Laser

The radio frequency carbon dioxide waveguide laser is not a new instrument. It was first introduced in 1978 by Macfarlane et al, at DREV.[1] Since then, almost every aspect of radio frequency (RF) CO_2 waveguide lasers has been examined. Early waveguide lasers were plagued by inefficiencies and low power output, but today moderate powers at acceptable efficiencies are attained. Today's demands for more powerful and compact lasers creates an interest in examining other laser discharge geometries. The slab laser is an attempt to increase the power output capability of RF CO_2 waveguide lasers while maintaining the compact form of the more conventional designs and reducing the cost and complexity of manufacturing.

Slab laser designs have been driven by the need to produce a 100 W laser suitable for surgical and light industrial use. Several related but less strict criteria have also influenced the design evolution. During this work, the general laser design complexity and fabrication costs were reduced over the current levels of CO_2 waveguide lasers. Ruggedness and durability were also improved compared to conventional waveguide lasers. The near field beam profile was to have a shape consistent with a single mode TEM_{00} beam, to ensure a symmetrical beam for delivery to the work area, while providing a beam that can be focused to tenths of a millimetre. By using these criteria a compact, inexpensive 100 W laser with good optical properties was constructed.

CO_2 lasers with 100 W outputs have been available for some time, but have distinct disadvantages over RF waveguide lasers; with the exception of two notable research efforts.[2,3] RF waveguide lasers are only beginning to approach

100 W capabilities. The comparable lasers in this power range are sealed, with no flowing gas, and have been both DC longitudinally and RF excited.

Sealed DC lasers are available with 100 W powers, but are large and fragile for the power they produce. DC waveguides, which have a greater power density, are only available in the 10 to 30 W range.[4] They use longitudinal excitation and have ignition voltages on the order of 1 KV/cm of discharge length. The high voltage present is an operational hazard. Modern high power (kilowatt and up) CO_2 lasers tend to be large and use forced circulation of the gas to maintain cooling.[46] Convective cooling has been the prerequisite for most moderate to high power lasers in use.

RF CO_2 waveguide lasers have several advantages over DC lasers. Inherently lower operating voltages (on the order of 150 volts) than the DC longitudinal discharge, create a safer instrument to operate. The lower operating voltage produces lower applied electric fields, improving efficiency by better coupling the excitation energy to the CO_2 molecules—improved E/P. Since the electric field can be applied transversely, the laser scales by current instead of voltage, simplifying scaling. A RF discharge has a positive impedance characteristic eliminating the ballasting resistors used in DC discharges. These are used to limit discharge current and control arcing. By eliminating them, further efficiency improvements are made, since power is not dissipated in the ballasting network.[5] Power can be capacitively coupled into the discharge, using RF, removing the electrodes completely from exposure to the gas plasma. This can lengthen the laser lifetime by limiting electrode degradation, but even when electrodes are in contact with the plasma, negligible sputtering of electrode material has been reported.[6] With these advantages, 18.7% efficient RF lasers have been constructed[7] without sacrificing a high power density. Power densities

as high as 0.84 W/cm of active length have been reported, higher than DC structures.[4] These advantages provide the ability to construct a small, rugged, and safe laser which is required for surgical, dental, and light industrial work.

Despite the beneficial characteristics of conventional waveguide lasers, they have many limitations when higher power is required and design complexity must be minimized. RF electromagnetic interference, thermal and optical damage are some of these limitations while others are more directly related to the active region geometry. The laser designs presented here are attempts to improve the thermal, optical, and discharge limitations in waveguide lasers.

The conventional CO_2 waveguide laser is constructed with a symmetric small bore ceramic waveguide which both contains the active region and forms part of the optical resonator. A vacuum housing encloses the guide assembly and positions the mirrors. Once the electrical tuning elements are included, the device contains many expensive and complex components.

Ceramic is used to construct the waveguide, because of its favourable optical properties at 10.6 μm. Alumina or beryllium oxide are the two most common, possess the lowest optical propagation loss, and have reasonable thermal conductivities when compared to glass or other similar waveguide materials.[8] BeO has the lowest optical loss and the highest thermal conductivity of the ceramics considered, but its dust is toxic and is not used by many investigators. Alumina has become the primary ceramic in use at the University of Alberta for these reasons. At discharge powers above half a kilowatt the ability of ceramic to conduct heat out of the discharge is not large enough to limit the operating temperature and maintain a high gain medium. The need to find a

material to have a low optical loss at 10.6 μm and have a good thermal conductivity is fundamental to the design of high power CO_2 waveguide lasers.

Ceramic–metal hybrid structures have been used,[9,5] but have shown greater thermal instabilities than homogeneous designs. This has led to many new waveguide designs which are all ceramic in construction.[10,11] Power scaling in a conventional waveguide laser is done by increasing the active region length. Ceramics of a length necessary to construct waveguide lasers with powers much greater than those found today are not readily available, but piecing the guide units together to form the needed active length introduces optical losses to the waveguide.[12] To construct a compact structure, the waveguide channel can be folded to contain the active region in a much shorter case length while trading the decreased length for an increase in bulk and width. Using an x-fold of the channels has produced 80 W in a 37 cm case length.[4] At optical powers of 100 W, the intracavity beam folding optics can be damaged from the intense fields present.[5] These properties form an upper limit on the power output capability of a folded waveguide laser. Using the small square bore ceramic waveguide for its superior properties places a limit on the maximum power output possible.

Some investigators have attempted to break away from the square bore waveguide to increase the power output. Xin and Hall[13] have developed a coaxial RF CO_2 laser that has produced 20 W at 7% efficiency, with 65 W at 9% efficiency recently reported.[14] This laser consists of two concentric aluminum cylinders which encase the active region. The optical resonator is constructed with a stable resonator using beam folding optics to repeatedly pass the beam around the cylindrical active region. Two properties of this design limit its usefulness to make a 100 W laser. Since the electrode separation is 8 mm, convective cooling is limited and scaling to 100 W would likely over–heat the

structure. Narrower electrode separations provide better cooling, but with a concentric design the parallelism necessary to obtain a low loss optical system is difficult to achieve. To optimally extract power from the discharge, the folding mirrors are designed to trade off maximum gain with the loss introduced with each pass. Increases in output power above 65 W have not been reported for this device.

Another departure from conventional design was taken by Newman et al.[3] is an arrayed waveguide laser similar to semiconductor diode lasers. The phased array waveguide laser has produced 95 W in a 37 cm long discharge, but with a near field beam 14 mm by 2.25 mm. This is the power target for the slab laser, but since the slab will be coupled into an articulated delivery arm, the near field beam profile requires symmetry. This minimizes high order mode generation in the delivery arm, and improves the delivered beam shape. The waveguide is an aluminum alumina composite. Aluminum creates a good heat sink, but the expense of machining the alumina to form the fine ridges needed for coherent operation is directly against the slab laser design basis. The far field beam contains 30% of the power in the side lobes which limits its usefulness. Binary phase gratings[15] have been shown to coherently combine the lobes to form a single beam, but such transformations occur in the far field while the near field is not changed appreciably which still creates an obstacle to coupling into a delivery system.

Jackson et al.[2] have developed a slab laser similar in design to the devices studied in this work; however, their research was conducted independently of the laser development done for this thesis. They have delivered 240 W in a 38 cm long active region, 4.5 cm wide, confirming the the slab technology to the 240 W

power level. Of the enhancements to CO_2 lasers discussed, the slab producing 240 W has proven that it is the most capable for further scaling to higher powers.

High power lasers require a robust RF delivery network. RF generators operate with a characteristic impedance of 50 Ω for most in common use, but the laser generally does not meet this condition. There is a need for an impedance transformation to maximize the power delivered to the discharge. A complicating factor is that discharge impedance is dependant on excitation frequency, gas pressure, gas composition, and power density.[16,5]

To optimize power transfer, the matching network must convert the load resistance to 50 Ω while bringing the reactive component to zero and dissipating as little energy as possible. Since the impedance is much greater before striking the discharge than after, the effect the network has on the open circuit voltage is important. It is desirable for the impedance transformation network to step up the open circuit voltage to aid in gas breakdown.[17] The discharge resistance falls to a constant value as power density is increased, causing the impedance match to change. For lasers that run at large discharge power densities, such as conventional waveguides, discharge resistance is constant over the operating region, simplifying the matching network. When power density is low, the resistance varies over the operating range creating difficulty in obtaining a wide impedance match to have optimum power transmission. The slab laser operates in the low power density region, compounding the difficulties in delivering a kilowatt while having little reflected power.

To form an efficient power transfer, the capacitance of the laser must be minimized.[18] This can be accomplished by resonating the laser capacitance out of the power delivery circuit.[5] Doing so lowers the resonant current in the matching network and lowers the thermal stress. Most matching networks are of a π–type

or L-type and use lumped components. At high powers the lumped components are under greater thermal stress which can limit the reliability of networks constructed with these devices. Other impedance transforming networks may be used to distribute the losses and lower the thermal effects. Two of these are quarter wave and coaxial stub matching networks which have distributed losses, but are much bulkier than a corresponding lumped network. For the slab laser, work was done to improve the delivery of kilowatt power levels into varying reactive loads while maintaining a low loss system.

The slab laser development has involved exploration into optical resonators, RF matching networks, and the construction problems of containing a kilowatt plasma in a small enclosure. There were two phases of development which were centered around the 3/30 cm laser, then the 5/30 and 6/30 cm lasers. The limits of the slab design were explored using the smaller 3/30 cm laser while the larger discharges were attempts to improve the performance defined by the 3/30 and meet the design goal of 100 W. Various parameters of the confocal resonators used were examined, but optics for the slab geometry remains the largest obstacle in optimization.

Chapter 2 describes the design basis of the slab geometry. This included optical, mechanical, vacuum, and electrical criteria required to create a 100 W laser. In chapter 3, the initial parameter optimization studies completed on the 3/30 cm slab laser are presented. Gas optimization was at the heart of this, but thermal and optical concerns were examined. The change from the 3/30 laser to larger active regions was made to overcome the inherent limitations of this device, and provide the required 100 W. Chapter 4 deals with the 5/30 and 3/60 cm lasers. The 100 W laser power goal has been achieved with the 3/60 cm slab laser while creating a design based on aluminum construction instead of the

standard ceramic. This minimized the complexity of the laser and reduced the construction cost.

Chapter 2: Slab Laser Design

All lasers have a set of fundamental components. For a CO_2 waveguide laser, the elements are the waveguide, optical resonator, excitation system, and vacuum chamber. The design goals presented in chapter 1 require the scaling of key laser components. This slab laser design introduces a new waveguide and optical resonator with the appropriate scaling modifications to the remaining elements.

Scaling the discharge region and waveguide to obtain greater power output required the introduction of a large mode volume optical resonator. To drive the laser to its fullest, a more robust electrical power delivery system was needed, along with a vacuum enclosure capable of containing and maintaining the laser over its intended lifetime. This chapter will introduce the slab laser design and the constraints created by the technology used.

2.1 Waveguide Design

Scaling of square bore waveguide lasers is accomplished by increasing the discharge length when the per unit length gain is optimized. With increased length comes greater guide transmission loss, forming an upper limit on the guide length and maximum power obtainable. The limitations of conventional square bore CO_2 waveguide lasers makes it necessary to look at new methods of scaling.

From the attempts of other investigators, and from trials of coaxial geometries in the Medical Laser Lab at this university, the prospective power scaling methods were reduced. A geometry where the discharge width is much

greater than its depth was proposed to sufficiently scale a laser to hundred watt capabilities. The square bore waveguide used in CO_2 waveguide lasers is shown as a cross–section in figure 2.1. It is constructed of metal and ceramic parts which contain the discharge in a small cavity and provide a waveguide for the intracavity beam. In figure 2.2 the basic slab waveguide cross–section is shown. The slab channel similarly contains the discharge and provides a waveguide. However, waveguiding occurs only in the narrow x dimension of the guide, unlike the square guide. The slab structure approximates an infinite planar waveguide when the sidewalls do not significantly interact with the optical beam[19] which is true for the devices under study. This planar waveguide allows the propagation of free space modes in the y dimension and a guided modes in the x dimension. The lack of waveguiding in the y dimension becomes both an asset and a problem when an optical resonator is chosen.

Waveguide propagation loss is an important factor in determining the operational efficiency of the laser. Ideally the guide should introduce no loss, but due to material constraints the waveguide can have a significant transmission loss. The rectangular waveguide propagation loss can be approximated by equations 2.1 and 2.2 as derived by Adams[20] and Laakmann[21] and modified for the notation in use here.

$$\alpha^{x}_{mn} = -\frac{n^2\pi^2}{2a^3k^2} Re\left(\frac{\nu_1^2}{(\nu_1^2-1)^{1/2}}\right) - \frac{m^2\pi^2}{2b^3k^2} Re\left(\frac{1}{(\nu_2^2-1)^{1/2}}\right) \qquad 2.1$$

$$\alpha^{y}_{mn} = -\frac{n^2\pi^2}{2a^3k^2} Re\left(\frac{1}{(\nu_1^2-1)^{1/2}}\right) - \frac{m^2\pi^2}{2b^3k^2} Re\left(\frac{\nu_2^2}{(\nu_2^2-1)^{1/2}}\right) \qquad 2.2$$

$$k = 2\pi/\lambda \quad , \quad \nu_i = n_i + jK_i \qquad 2.3$$

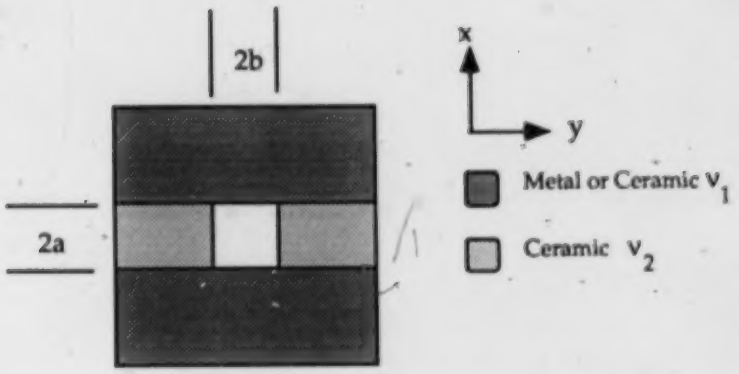

Figure 2.1 Cross–Section of Rectangular Waveguide

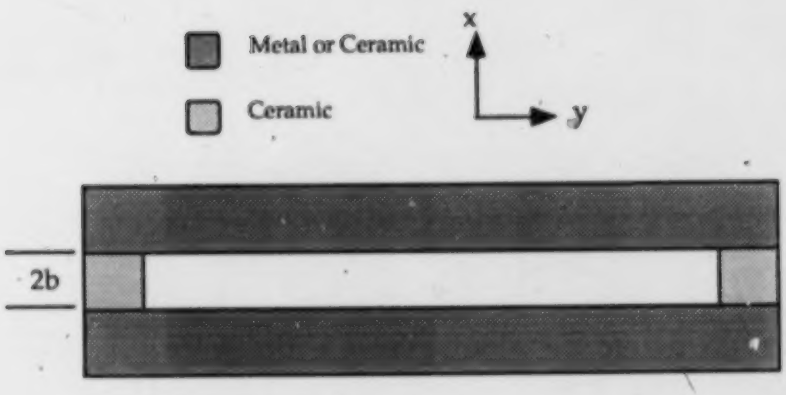

Figure 2.2 Cross–Section of Slab Waveguide

The propagation loss, α from the X or Y polarized waves in the symmetrical guide, is dependant on the material's complex refractive index, ν. The complex refractive index is composed of the refractive index n_i, and the extinction coefficient K_i. The loss for both a TE and TM wave, which are components of the hybrid electric mode EH_{mn}, are the constituent terms in equations 2.1 and 2.2. When $a \gg b$, the beam side wall interaction becomes insignificant, and waveguiding can be ignored in that plane. For metal electrodes with $\nu \gg 1$, and $a \gg b$, α reduces to:

$$\alpha_m^{TM} = \frac{m^2 \lambda^2}{b^3} Re(\nu) \qquad 2.4$$

$$\alpha_m^{TE} = \frac{m^2 \lambda^2}{b^3} Re\left(1/\nu\right) \qquad 2.5$$

Two wall guiding introduces less propagation loss than the four wall case for a given wall material based on equations 2.4 and 2.5. For aluminum[1] at 10.6 μm $\nu = 27 - i70$, and with a ten times larger than b, the propagation loss coefficients are given in table 2.1.

Table 2.1 Propagation Loss Coefficients

	α^{TM} (m^{-1})	α^{TE} (m^{-1})
Al_2O_3 from ref. 5 $\nu = 1.15 - j0.0144$	2.3×10^{-2}	1.74×10^{-2}
Aluminum $\nu = 27 - j70$	2.66×10^{-1}	4.73×10^{-5}

From the table, the dominant, lowest loss, mode will be the aluminum TE mode. Based on the propagation loss, aluminum is the preferred construction material for the waveguide. However, published accounts[19,22,23] have shown that the value of ν quoted in the literature is not a reliable value, since the natural aluminum oxide covering and the polycrystalline nature of commercial aluminum are not taken into account. Further, waveguide surface roughness increases the actual transmission loss[24,19] leading to an optimistic loss calculation, when equations 2.1 through 2.5 are used. Table 2.1 does not give absolute loss numbers but provides a loss trend when surface effects remain constant. The finish of the 1/30 and 3/30 cm laser waveguides was completed on the micro-surface lathe to minimize the surface irregularities, and to lower transmission losses. Surface finish of the 3/60 slab was improved after machining by hand polishing with a commercial metal polish.

Equations 2.4 and 2.5 show that TE mode propagation will be the low loss mode in a slab waveguide for materials at 10.6 μm. Unlike square homogeneous waveguides which have no preferred polarization axis, the slab will be polarized normal to the waveguide surfaces. The known polarization vector can be of use in low loss coupling of the laser into a flexible waveguide delivery system.[19,22,25]

Aluminum has been selected for use as the waveguide channel for several reasons. As shown in table 2.1 aluminum has the lowest propagation loss of the available materials. It is inexpensive to machine into the desired forms, in comparison with alumina. Thermal conductivity is comparable to copper and better than alumina. (See table 2.2 for a comparison of thermal conductivities.) Using a metal instead of a dielectric eliminates the need to plate the dielectric to form an electrode, reducing the construction complexity, and improving the

Table 2.2
Thermal Constants of Waveguide Materials[1]

Material	Thermal Conductivity cal/cm•sec°C @ 20°C
BeO (high purity)	0.58
Alumina (99.5% Al_2O_3)	0.047
Al	0.57
Cu (99.9%) †	0.918 @ 18°C 0.908 @ 100°C

† Copper is included to represent a good thermal conductor only and is not intended as a waveguide material.

structural integrity. Discharge powers of 1000 W require an extremely robust electrode to prevent damage.

2.2 Vacuum Enclosure

The laser must have a vacuum housing to maintain the appropriate gas balance for laser action to occur. The choice of this enclosure has implications for the electrical excitation system and the optical system to meet the design specification. Two vacuum housings have been developed to meet the experimental requirements. A general purpose box used for the preliminary work was constructed first, followed by a specific enclosure for the 3/60 laser. The general requirements for the laser vacuum chamber will be discussed here with the details of the 3/60 housing covered in chapter 4.

The waveguide/electrode assembly, formed by aluminum plates and alumina spacers, was mounted in an aluminum box as shown in figures 2.3 and 2.5. The box forms the vacuum envelope and the cooling system. It was designed for flexibility and ease of use as a general purpose experimental laser housing such that it would be simple to make small changes in the lasers without a major refit. With the simplicity of the slab laser most of the work involved with the laser assembly is in the vacuum enclosure and the necessary optical, RF, and cooling feedthroughs.

Cooling the gas is essential for any laser action to take place. Carter and Marcus[12] have found that a 10°C drop in the channel temperature results in a 20% increase in laser power. The slab laser housing has a plate located at the top and bottom of the vacuum enclosure to create even cooling (see figure 2.4). Tap water was used as the cooling medium as it was readily available. The waveguide makes a press fit between the bottom of the enclosure and the lid,

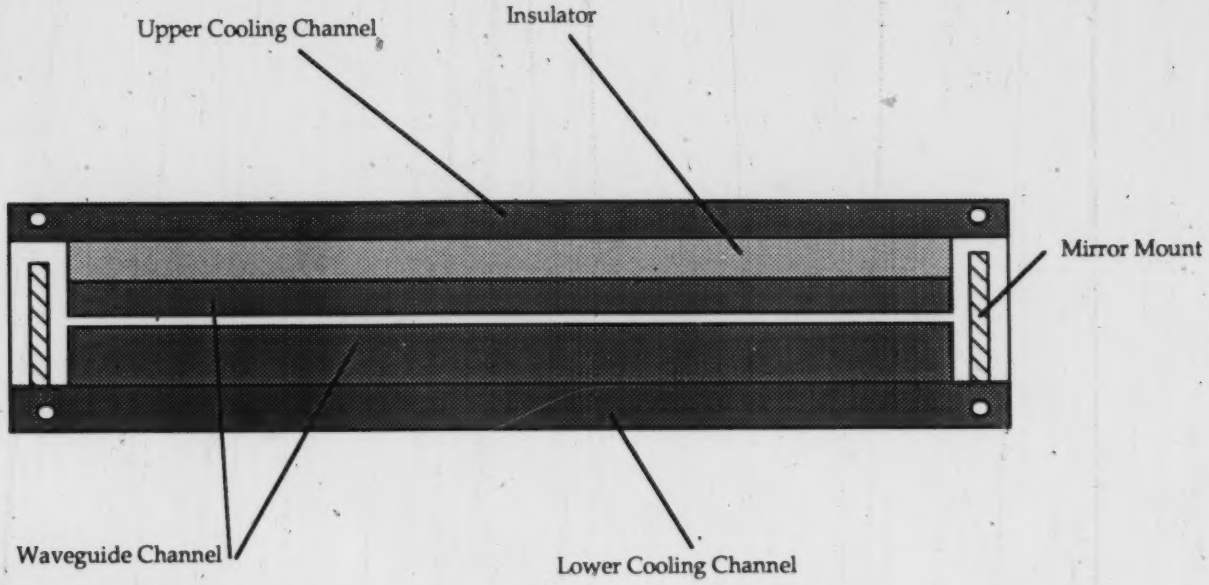

Figure 2.3 Slab Laser Cross-section

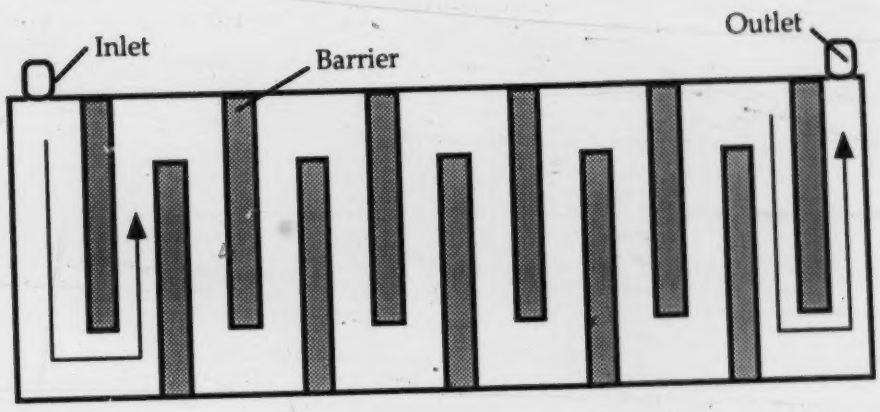

Figure 2.4 Cooling Channel Plate Cross–Section

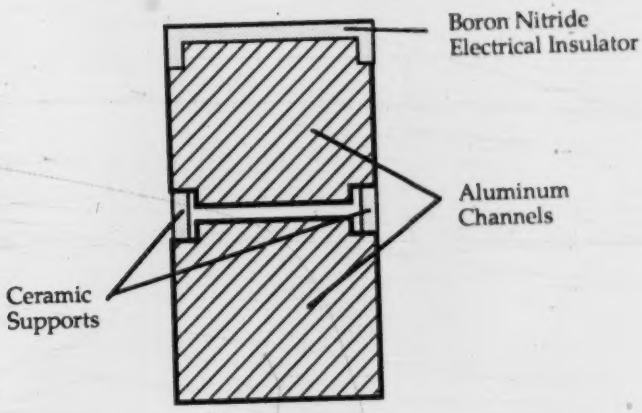

Figure 2.5 Slab End Cross–Section

with water passed through the lid and the bottom plate. Cooling of the plasma is made through conduction by the aluminum channels forming the waveguide. This created a good cooling scheme at powers of several hundred watts, but the boron nitride electrical insulator used to separate the powered (hot) electrode had too much thermal resistance (see chapter 3 for details), and the channel became too warm under operation.

The final elements of the laser housing consist of the feedthroughs. Optical feedthroughs were made with antireflection coated ZnSe windows of $^3/_4$ in. diameter. They, one at each end of the laser, were held in place by a threaded plastic ring and o-ring which screwed into the end walls of the housing forming a vacuum fit. The RF feedthrough was made of a $^1/_4$ in. diameter threaded copper rod Torr–Sealed into a hollow alumina dowel. Torr–Seal is a low vapour pressure epoxy resin commonly used in vacuum systems. This assembly was then held into the housing and formed a vacuum seal with a swagelok bulkhead fitting. Contact with the channel and RF feed is formed by screwing the copper rod into the side of the top (hot) channel, forming a solid connection.

Design constraints created by the vacuum housing complicate the optical design and the electrical system. Mirror mounts had to be designed around the physical constraints of the space left after a given electrode assembly was in the enclosure. Feedthroughs for the translational stages on the mirror mounts were further constrained by the cooling system. The voltage balancing network had to fit in the vacuum housing, since feedthrough distances were too great to resonate the electrode assembly from outside the chamber. This complicates the voltage balancing of the laser since it cannot be done under operation. The simple vacuum chamber can place serious restrictions on the laser components.

2.3 Resonator Design

The broad geometry of the slab discharge causes difficulty in coupling the active region into a beam with suitable properties as outlined in chapter 1. There are three categories of optical resonator that were considered. Of these three types, free space stable resonators are the least suitable for two reasons. Primarily, they are difficult to construct when a large modal cross–section is required, as in this case. The second difficulty is the interaction with the narrowly spaced electrodes. For reasons of cooling efficiency it is not desirable to widen the electrode spacing. This causes unacceptably large intracavity transmission losses due to the free space modes interacting with the electrodes. To circumvent these losses, it is necessary to use a waveguide resonator in the narrow discharge direction.

In conventional waveguide lasers, plane–plane optics have been used with modal stability being maintained by the waveguide. A plane–plane resonator can provide a low order beam in the narrow x guide dimension, but high order modes are present in the wide y dimension. Since the waveguide does not limit the beam to the lowest order mode in the y dimension, a resonator must be chosen that does. A second difficulty in using a waveguide resonator is the transmissive optics needed must have a high damage threshold to withstand the expected optical power densities of 100 W/cm^2 or more. With the slab's wide active region, transmissive optics are prohibitively costly and create a very thin and wide beam. This laser beam does not lend itself to coupling into existing delivery systems,[26] and without cylindrical optics to transform it into a symmetric beam, is not appropriate for use in surgical or dental procedures. The problem then is to construct a resonator that has a large mode volume which

emits a small symmetric beam. This can be achieved with a confocal unstable–stable resonator.[27]

Table 2.3
Advantages of The Confocal Unstable Resonator[28]

- Large mode volume.
- Controllable diffractive output coupling.
- Good transverse mode discrimination.
- Single–ended all–reflective optics.
- Collimated output.
- Efficient power extraction.
- Good far–field mode pattern.

The useful extracted energy from an unstable resonator is from diffraction of the internal optical field past the mirror edges, rather than propagation of the beam through a partially reflecting mirror. An unstable resonator has a divergent solution to the equations governing the propagation of rays through the equivalent periodic lens guide for the resonator, hence its name.[29] A confocal unstable resonator has been chosen because of the beneficial properties outlined in table 2.3. The chosen resonator operates in the upper right hand quadrant of the stability plane, the positive branch. Figure 2.6 shows the general resonator stability diagram. A positive branch system was chosen because the negative branch resonators have an intracavity focus that can adversely affect the gain region and laser performance. Figure 2.7 is a diagram of the confocal resonator. From figure 2.7 the stability parameters g_1, g_2 can be found were L is the resonator length and R_i represents the i_{th} mirror radius—taken positive with concave surfaces, then[30]:

$$g_i = 1 - \frac{L}{R_i}, \text{ with } i = 1, 2. \qquad 2.6$$

$g_1 g_2 \leq 0$, unstable negative branch. 2.7

$g_1 g_2 \geq 1$, unstable positive branch. 2.8

Unlike a stable resonator, the unstable resonator output coupling is controlled by the magnification of the mirror system (see table 2.4).[28] The resonator coupling can be calculated from the ratios of the transmitted beam to the overall resonator width. This is only a first order geometrical approximation, but does provide a physical understanding and gives a reasonable starting point for the optimization of the laser.

Unstable resonators are not readily applied to the slab geometry, since this geometry has wide but narrow cross–section, and an intracavity waveguide. For optimal coupling into the waveguide, cylindrical optics are necessary to maintain low diffractive losses, while creating the unstable resonator in the wide dimension. A stable–unstable resonator was used by Bourne and Dyer[27] in an KrF laser, but is too costly to construct based on the design specifications. As Bourne's resonator is not a waveguide–unstable system it is not directly applicable to this work, but does show that such systems are technically feasible with unstable resonators.

By using a waveguide–unstable resonator, the large mode volume can be fully exploited while the coupling loss in the waveguide is minimized. It is necessary to use one of the low loss coupling conditions to minimize the diffractive loss from the waveguide modes past the mirrors and the loss associated with the free space mode re–entering the guide. The two simplest low loss solutions are flat mirrors placed on the ends of the guide, or concave mirrors placed such that the distance to the waveguide is equal to the radius of curvature.[31] This would indicate that cylindrical optics are needed to mount the

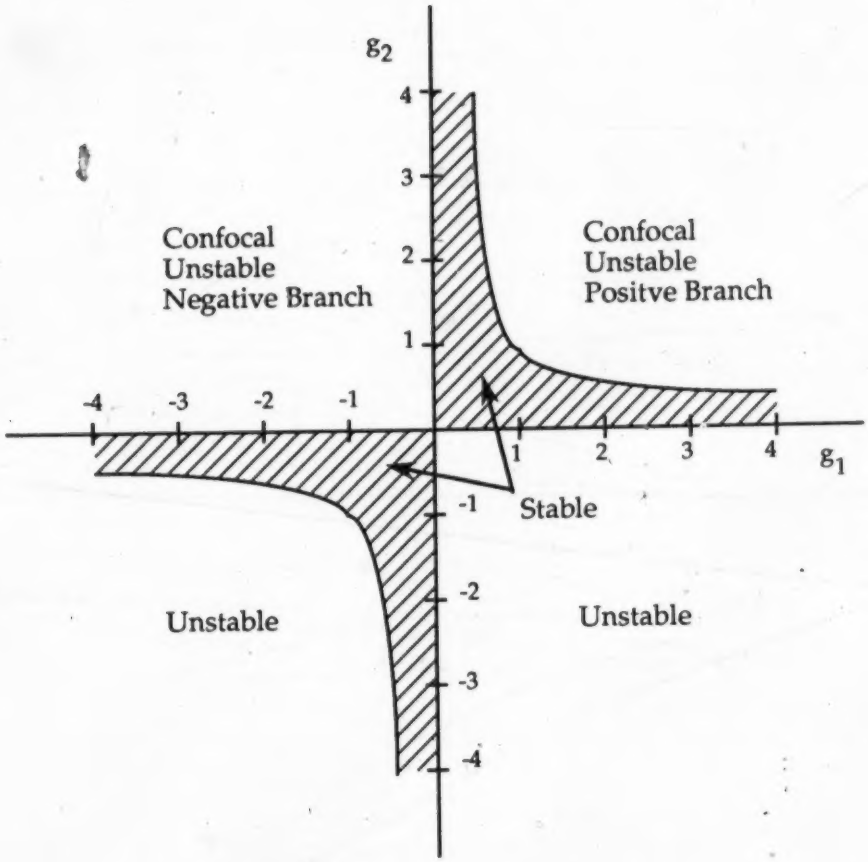

Figure 2.6 Optical Resonator Stability Diagram

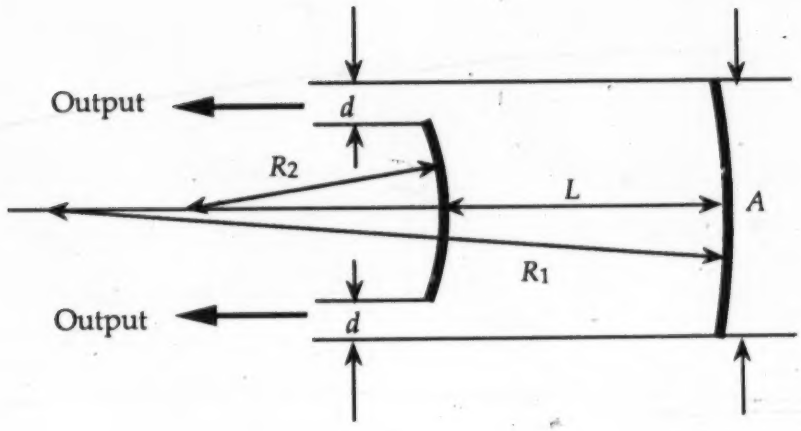

Figure 2.7 Confocal Unstable Resonator

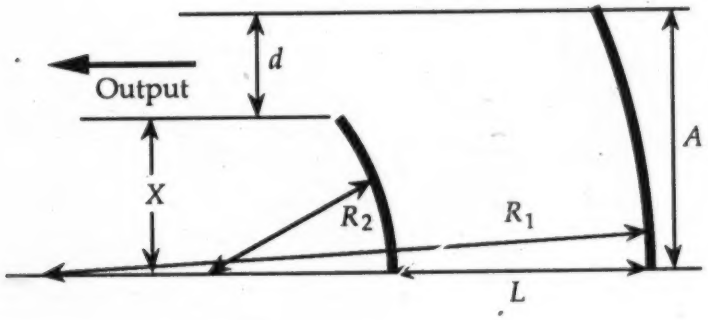

Figure 2.8 Off Axis Confocal Resonator

mirrors close to the guide, but if the curvatures used for the unstable resonator are large enough such that they can be treated as flat, then spherical mirrors can be used. Spherical mirrors are easier to construct and consequently less costly.

The one dimensional or strip confocal resonator in figure 2.7 shows the dual output beams typical of the centred output mirror. This is not desirable. It is not possible to couple the dual beams from the near field of the flat confocal resonator into existing delivery systems. With the off-axis operation (figure 2.8), the near field is a single uniform beam as opposed to the two sections that form the standard output of an unstable resonator. In the geometric limit, the near field of this off axis resonator has a uniform magnitude and phase over the output opening. Having a solid near field pattern is useful for transmission into the delivery arm, and in transmission through the vacuum enclosure since only one ZnSe window is needed. It was found by Sutton[32] et al. that using a noncentered output mirror causes more energy to be coupled into the center lobe of the far field pattern than is the case with centered output mirrors. With no added difficulty in construction or operation, the beam properties needed to meet the design goals are achievable with an off axis unstable resonator.

To construct an off axis resonator, the centered output mirror of figure 2.7 is turned until the optical axis approaches one edge. All design equations and construction principles of the centred confocal resonator apply for this design. The off axis resonator will provide the same geometric coupling as the centered resonator, and will not deviate in any other fundamental aspect, except the diffraction details of the mode shapes and volumes.[28] A change in the resonant modes from the waveguide resonator to the unstable system will modify the power extraction of the laser, from this case. The change in power extraction is dependant on the diffractive properties of the particular optical cavity.[30]

Table 2.4
Confocal Unstable Resonator Parameters[28]

Coupling (X is the front mirror width):

$$\delta = 1 - \left|\frac{1}{M}\right| = 1 - \frac{X}{A}$$

Magnification:

$$M = -R_2/R_1$$

Radii:

$$R_1 = -2L/(M-1), \qquad R_2 = 2ML/(M-1), \qquad M > 1 \text{ or } M < -1$$

Output beam width:

$$d = A\,\delta$$

Confocal equation:

$$R_2 - R_1 = 2L$$

The slab laser has a low gain per unit length, based on the similarities of the active region in conventional waveguide lasers and the slab laser. A low gain laser requires a small percentage coupling to optimally extract the power. A value on the order of 10% is quite typical of CO_2 waveguide lasers.[5] The initial coupling, δ, was based on the formation of an output beam, 1.88 mm wide by 2.25 mm high, from a discharge width of 30 mm. This gave a δ of 6.3%. As an initial approximation it produced a coupling in the required range and a useful output beam profile.

By using the required coupling and discharge dimensions in the equations of table 2.4, the magnification of the confocal resonator is 1.067. This results in R_1 = -9.0 m, and R_2 = 9.6 m. The resultant stability coefficients are 1.033 and 0.969 giving a product of 1.001, which is very close to being a stable plane–plane resonator. This would indicate a mechanical stability problem during operation, as alignment is very critical.

Mirror radii for the unstable resonator, designed above, are long and can be considered flat for waveguide coupling purposes. Flat mirrors form a low loss system with the waveguide when placed against the guide. The mirrors cannot be positioned on the guide ends, nor can they be placed within several millimetres, since both interaction with the plasma and particle damage will limit their useful lifetime. Therefore, the mirrors were placed as close as possible to the guide without gas breakdown occurring to the mirror. This was 5 mm which was dependant on the applied RF power and the gas pressure.

With the mirrors at a distance from the guide, coupling loss will occur, lowering the laser efficiency. Coupling efficiency of the resonator mirror waveguide system, for a square waveguide, is given by Prunty[31,14]:

$$|A_{00}|^2 = \frac{4\alpha^2}{\left(\alpha^2+4\beta^2\right)\left|\alpha^2+4(1-\beta)^2\right|} \qquad 2.9$$

$$\alpha = \frac{k\,\omega_0^2}{c}\ , \quad \beta = d/c \qquad 2.10$$

$$\frac{\omega_o}{a} = 0.7032\ , \quad k = 2\pi/\lambda \qquad 2.11$$

, where d is the mirror guide separation

, c is the mirror radius

, and a is the waveguide radius.

Where $|A_{00}|^2$ is the fraction of the energy coupled into the fundamental mode when the fundamental mode is emerging from the guide. Equation 2.11 represents the ratio of free space beam waist to guide aperture that maximizes the power coupled into the fundamental mode. Equation 2.9 will only give an approximation to the coupling losses for the slab waveguide, but is useful for a physical understanding of the problem. Based on equations 2.9 to 2.11, the coupling loss for a 10 m radius mirror placed within 5 mm of the guide is approximately 0.1%. The power lost while the beam is exiting and re-entering the guide is small, based on equation 2.9, so the mirror placement should not contribute significant loss to the round trip cavity losses.

An off–axis stable–unstable optical resonator, fashioned using a waveguide, can produce the desired beam properties. It is only a minor deviation from the centred resonator and can be constructed with long radius spherical mirrors. The large mode volume will effectively extract power from the active region contained between the waveguide/electrode plates.

2.4 Electrical System

The RF power delivery network is made up of several sections as shown in figure 2.9. In general the RF network consists of a power supply, power metering, delivery coax cable, matching network and the laser under test. Matching networks formed the bulk of the work on the electrical delivery system, as previous designs did not have the power handling capability needed.

The excitation frequency is constrained by physical and mechanical limits. A fundamental lower limit on frequency of 20 to 30 MHz exists due to electron loss into the channel walls, causing discharge instabilities,[5] with a practical upper limit of 150 MHz, due mostly to component values and the tolerances involved in working at this frequency. A 1000 W 72 MHz RF power supply furnished the drive for the laser, as this was available in the lab. The frequency of 72 MHz has been standardized on by this lab over the last five years, and is relatively easy to work with. He and Hall[33] indicated that there is a frequency dependence on the discharge resistance, which influences the discharge voltage and the E/N ratio. Since there is a direct influence on the E/N ratio by frequency it should be explicitly optimized for each gas mixture, pressure and electrode design. However, this was not possible due to lack of access to a broad band tuneable RF power supply.

RG–213 was chosen for the delivery cable, since it is low loss and has a 12 AWG stranded core, which would better stand the power loading of 1000 W. An N–type RF connector was chosen to handle the power requirements, as BNC connectors repeatedly failed.

The laser does not have a 50 Ω impedance under operation, thus imposing some form of impedance matching network for optimum power transfer. It is

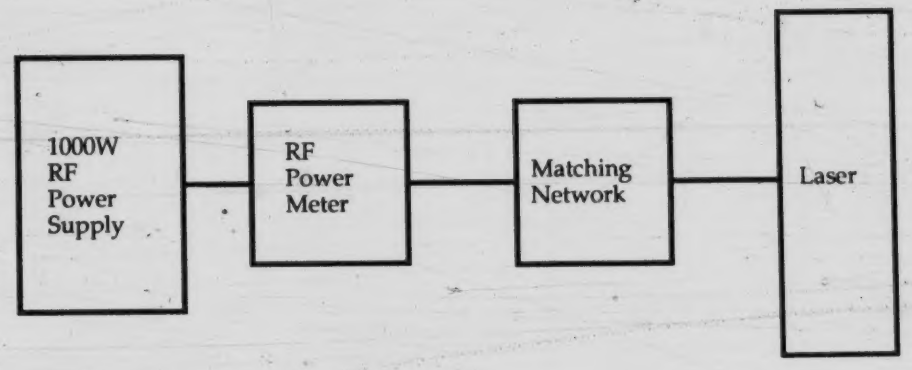

Figure 2.9 Experimental Electrical Network

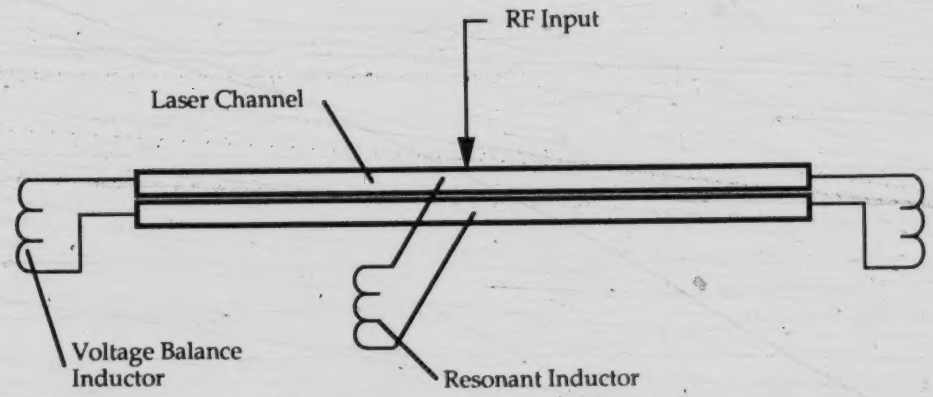

Figure 2.10 Voltage Balancing Inductors

known that the resistance of the square bore waveguide laser of similar length is approximately 600 Ω.[17] By scaling the discharge width from equation 2.12 the expected resistance for the slab laser can be found.

$$R_d = \frac{m \nu d}{n e^2 A} \qquad 2.12$$

$$R_d \propto \frac{1}{A} \qquad 2.13$$

If the remaining terms are constant, with A being the discharge area, scaling to a 30 mm wide discharge produces a discharge resistance, R_d = 40 Ω. This is sufficiently close to 50 Ω to not use a matching network, at least for the initial experiments. It was found that the discharge impedance dropped sufficiently above 500 W, and that a matching network was necessary for operation above this power. The discharge impedance drops to approximately 25 Ω in this region, making a conventional discrete matching network difficult to construct for use with kilowatt RF levels. The matching network was formed by paralleling two $\lambda/4$ RG–11, 75 Ω cables, creating an impedance transformer with a 25 Ω load impedance. These simple methods have worked well, but do not allow a very close match since they are not adjustable during laser operation. A tuneable matching network was developed for use with the 3/60 laser and will be elaborated on in chapter 4.

The final element of the electrical network is the laser, which has several undesirable electrical properties. The laser is capacitive which complicates matching, and transmission line effects induce voltage imbalances along the discharge length. These effects must be minimized to construct a high efficiency laser.

Transmission line effects have been reported by several investigators[3,4,5] in the voltage distribution along the length of an RF waveguide laser. To maximize the laser gain, it is necessary to make the channel voltage uniform. In practice, this results in minimizing the voltage variations to less than 5%. To achieve this, inductors are placed along the length of the guide to adjust the voltage. In long dielectric channels the electrical length can be appreciable in comparison with the RF wavelength in use, but with the aluminum channels the electrical length is much less, thus requiring fewer inductors to smooth the voltage.

Channel capacitance can be removed by resonating the electrode structure with inductors. This is done by adjusting the inductors along the length of the laser channel and by adding a trimming inductor to resonate the channel.

$$F_0 = \frac{1}{2\pi\sqrt{C_l(2L_b + L_r)}} \qquad 2.14$$

Were F_o is the resonant frequency, L_b is the combined voltage balancing inductance, L_r is the resonant trimming inductance, and C_l is the lumped channel capacitance. Doing so leaves the dischargeless laser a resistance at the resonant operating frequency. It is then only necessary to match the discharge impedance to the supply with the matching network.

For the slab lasers a total of three inductors are used to balance the voltage and resonate the structure. They were calculated, as an initial approximation, by equation 2.14 assuming a lumped capactive element formed by the channel and divided into three equal inductances. A low level reference voltage is applied to the channel with it in the vacuum housing, to include the parasitic capacitances of the case. The end inductors were then adjusted to optimize the balance, with

the central inductor being adjusted to compensate for the channel resonance. This procedure provided a voltage variation of less than 5%.

Chapter 3: The 3/30 Slab Laser and Optimization

The first laser tested had a 3 cm wide by 30 cm long slab discharge. Characterization and optimization of the 3/30 laser was completed with the immediate goal of producing a 100 W laser, based on discharge area scaling. However, 100 W from this laser was optimistic, as 50 W was the maximum obtained.

For the laser optimization to be conducted, an experimental test bench was constructed. This included the RF drive, gas handling, optical power metering, and a beam profile measurement system. Experiments conducted with the 3/30 slab laser were made with a flowing gas system. The following sections explain the test bench, experiments, and the optimization that was conducted on this version of slab laser.

3.1 Experimental Test Bench

The experimental apparatus for the testing and optimization experiments consisted of the laser optical system, gas handling system, cooling, and the RF network. Figure 3.1 displays the basic optical experiment bench. A Coherent model 201 thermal power meter was used for laser output power measurements. The power meter electronics are seen in the foreground of figure 3.1. Figure 3.2 shows the flowing gas control station, and the RF power supply, a Henry Linear model 1000D.

Figure 3.3 is the basic block diagram of the vacuum and cooling systems. Tap water was used as the cooling medium with tap outlet temperatures varying from 18°C in July/August to 12°C in January/February. 3:1:1 (He:CO_2:N_2) was

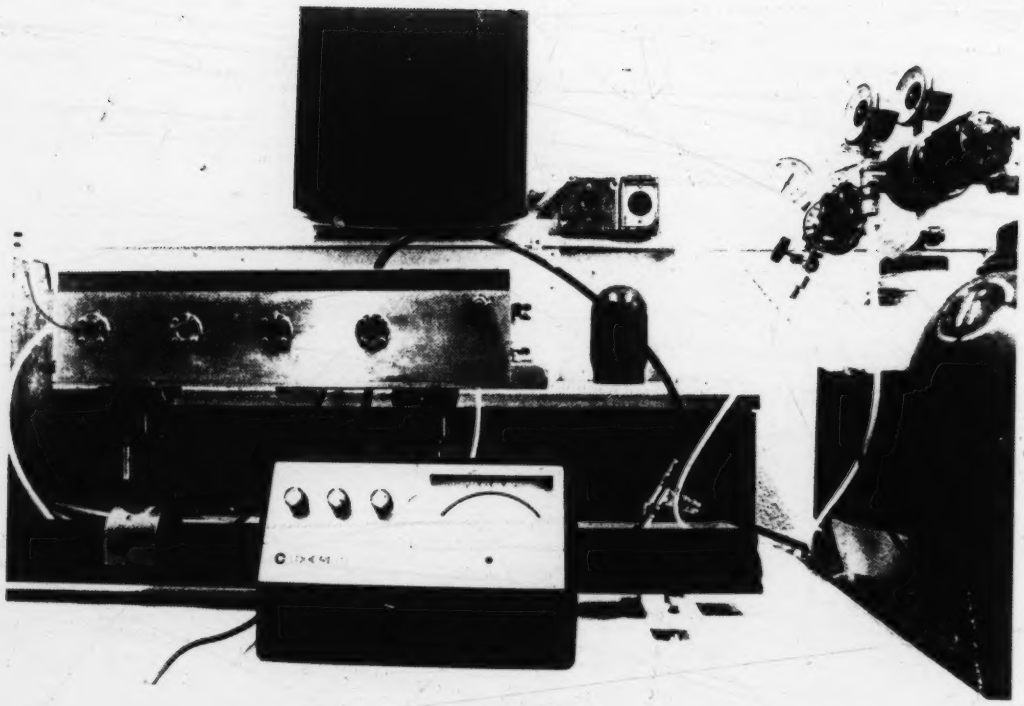

Figure 3.1 1 cm and 3 cm Slab Laser Vacuum Housing

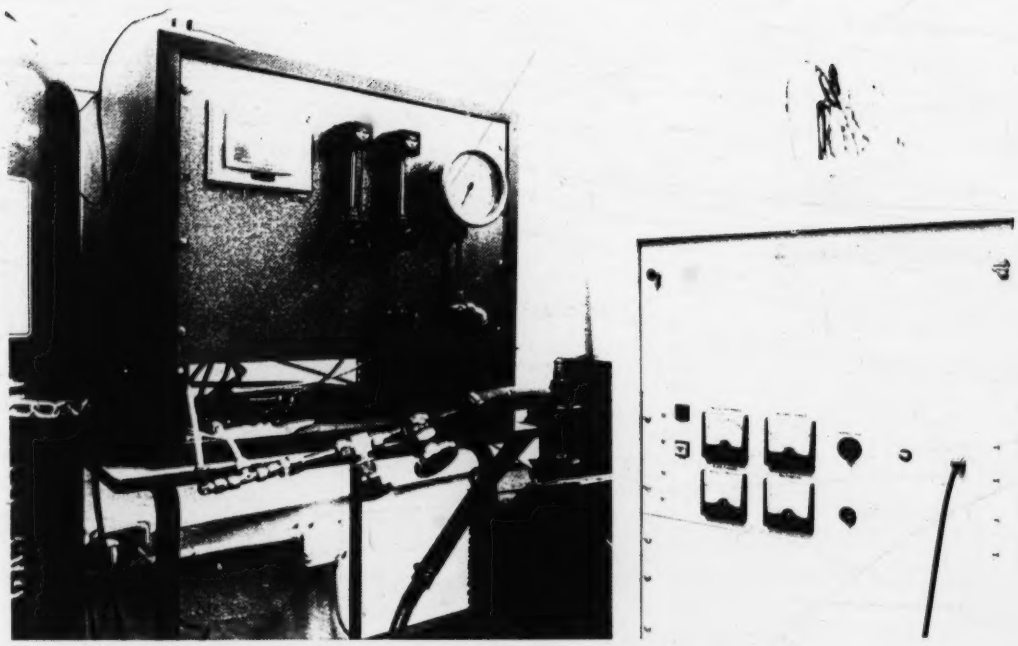

Figure 3.2 Flowing Gas Vacuum System and Kilowatt RF Power Supply

available as a premixed gas and was used as the primary supply, with dilutions made by mixing with helium. Flow rates and mixture was controlled by two rotameter flow meters, symbol FE in figure 3.3. This system enabled the flow rate, mixture, and laser pressure to be set independently, while the laser was in operation.

To simplify the initial laser testing, a slow flow gas system was used. The slab laser will be operated under sealed conditions (no net gas exchange) in its final form, and in an attempt to furnish an operating environment similar to this a low flow rate was used (approximately 1 litre/minute). Using a flowing gas system further simplifies mixture dilution, as 6:1:1 ($He:CO_2:N_2$) can be made simply from 3:1:1 ($He:CO_2:N_2$) without the need for mixing tanks and the delay involved while the gas comes into equilibrium. A mass flow controller could be used for mixture control, but was not available. By using low flow, the flow induced laser end to end pressure drop was reduced, while the cooling from the flow was minimized. A flowing system permits less stringent vacuum material requirements than the no flow case, since contaminants outgassed in the gas handling system and laser are flushed out, rather than building up. Stability of the gas pressure was a problem and was constantly monitored during experiments as it would drift from the preset conditions, and introduce laser power variations. This laser test bench was easily refitted for further experiments and provided the necessary flexibility and controls.

3.2 Parameter Study and Optimization

The basic premise was to optimize the 3/30 slab laser to achieve a 100 W output. As stated this laser never produced more than approximately 50 W once optimized. It has been observed by Lavigne et al.,[35] and Sinclair[5] that an optimum pressure and gas mixture exists to balance the total distributed losses in

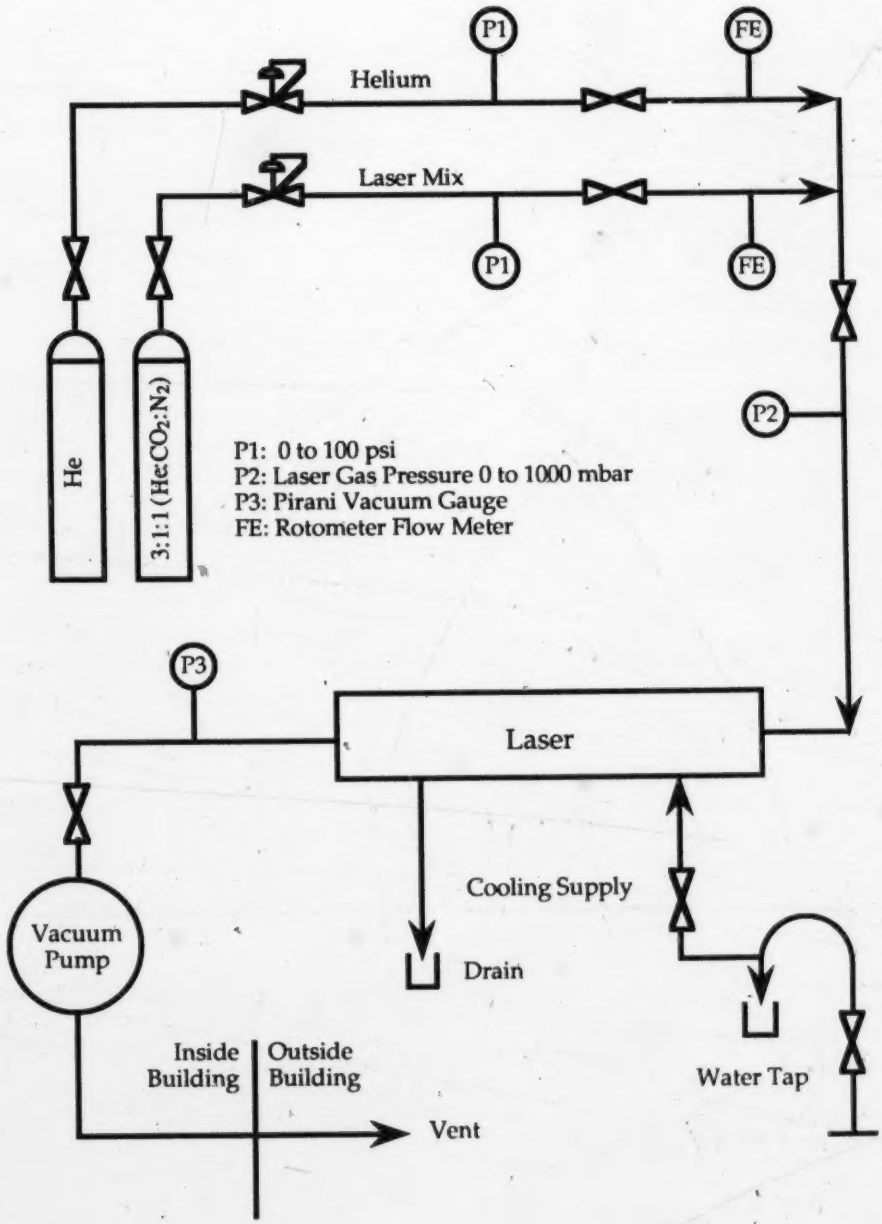

Figure 3.3 Flowing Gas Vacuum System and Cooling Piping Schematic

the laser. Optimization was carried out by maximizing the laser output for both gas pressure and mixture.

In the pressure broadened regime Rigrod's[36] gain equation indicates the power per unit length is proportional to the square of the mixture pressure. This creates the most power at the highest possible pressures. However, from Rigrod's equation:

$$P_0 = I_s \alpha_0 L\, A\, B \left(1 + \frac{\ln\sqrt{R_2}}{\alpha_0 L}\right) \qquad 3.1$$

$1 + \frac{\ln\sqrt{R_2}}{\alpha_0 L}$ is the extraction efficiency.

In equation 3.1 R_2 is the output coupling fraction, α_0 is the gain, I_s is the saturation intensity, A is the mode cross–sectional area, B is the collected losses, and L is the active length. Since both the total power and the extraction efficiency are functions of the gas parameters, the maximum obtainable power output is dependant on the choice of these parameters.

The optical resonator in use for these tests was the –9.0 m and 9.6 m set designed in chapter 2. This set of mirrors had a geometric coupling of 6.3%. No changes were made to the mirrors during the course of the gas tests. RF power was limited to 500 W P_d (net discharge power). Above this point the laser became increasingly unstable: its ability to stay in a single waveguide mode was reduced, and the repeatability of results above 500 W P_d was questionable. This was one of the primary reasons in failing to achieve 100 W optical power levels with this laser.

For discharge powers less than 500 W, the laser impedance was close enough to permit direct coupling without an impedance matching network. As the power density increases, the discharge resistance falls;[17] with a fixed

matching point of 50 Ω at powers above 500 W with 3:1:1 ($He:CO_2:N_2$) the discharge resistance had dropped below 50 Ω causing the reflected power to increase. Above 500 W, the 28 Ω quarter wave impedance transformer was used as it had a better match to the laser. A variable matching network was not developed until work on the 3/60 slab began, since the 3/30 laser operated sufficiently close to the impedance provided by the fixed matching networks that it was not required.

The first parameter tests consisted of the variation of gas pressure for a constant gas mixture. Gas pressures from 40 torr to 120 torr were used with constant discharge powers of 200, 300, 400, and 500 watts. Discharge power was not set directly, but forward power was, and then the reflected power was accounted for. For comparison, it is desirable to keep the discharge power levels as constant as possible over the gas tests to allow for comparison over varying mixtures. The gas pressure experiment was conducted for 3:1:1, 4:1:1, 6:1:1, and 8:1:1 ($He:CO_2:N_2$). Figures 3.4 through 3.7 show the effect of these experiments on the laser power.

From these figures some trends can be seen. For a given gas mixture there exists an optimum pressure that maximizes the extraction efficiency at a particular discharge power. The optimum pressure increases with applied RF drive. This is consistent with the literature.[35,7]

The small variation in the discharge power (1% to 8%) was caused by power fluctuations in the RF drive during the tests. The RF amplifier decreased the drive as it became hot under operation, which caused variations in the discharge power over the course of an experiment if left unchecked. This caused variation in the net power delivered to the laser and was noted on each power curve.

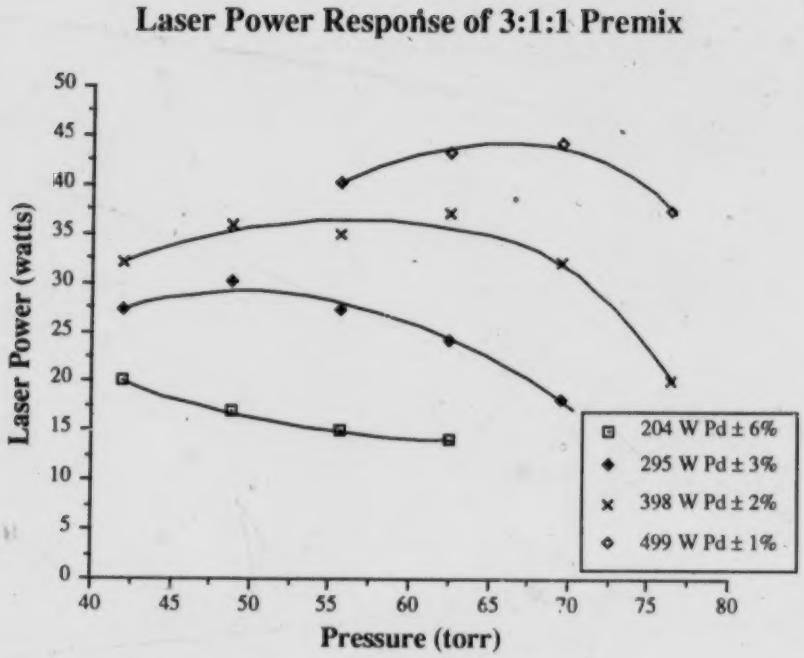

Figure 3.4 The change in laser power for variations in gas pressure for 3:1:1 ($He:CO_2:N_2$)

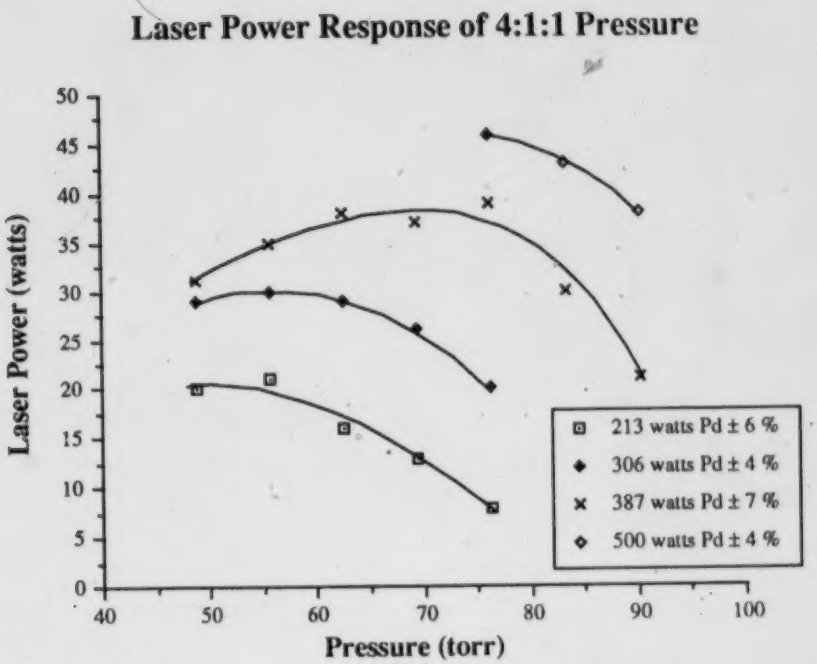

Figure 3.5 The change in laser power for variations in gas pressure for 4:1:1 ($He:CO_2:N_2$)

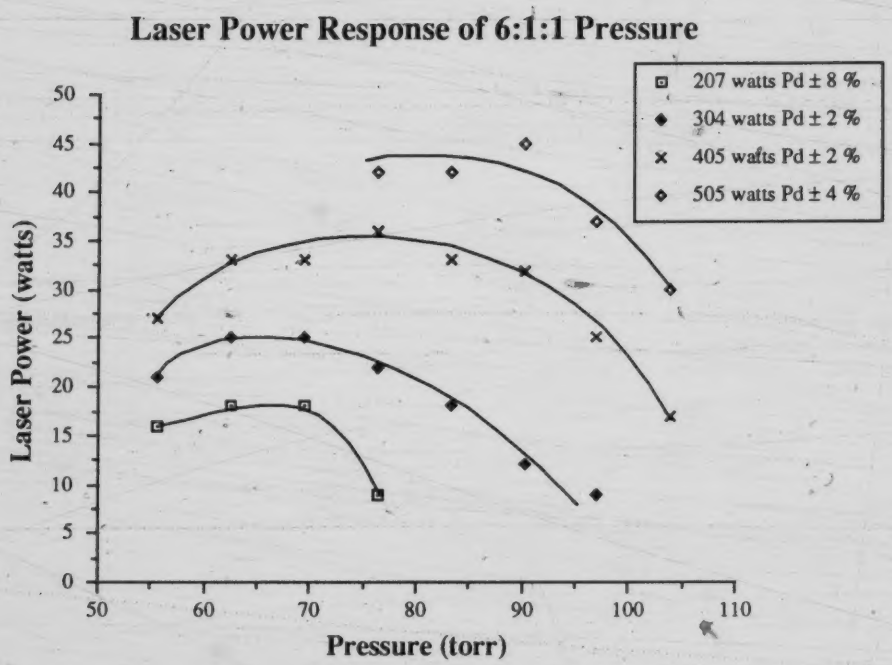

Figure 3.6 The change in laser power for variations in gas pressure for 6:1:1 ($He:CO_2:N_2$)

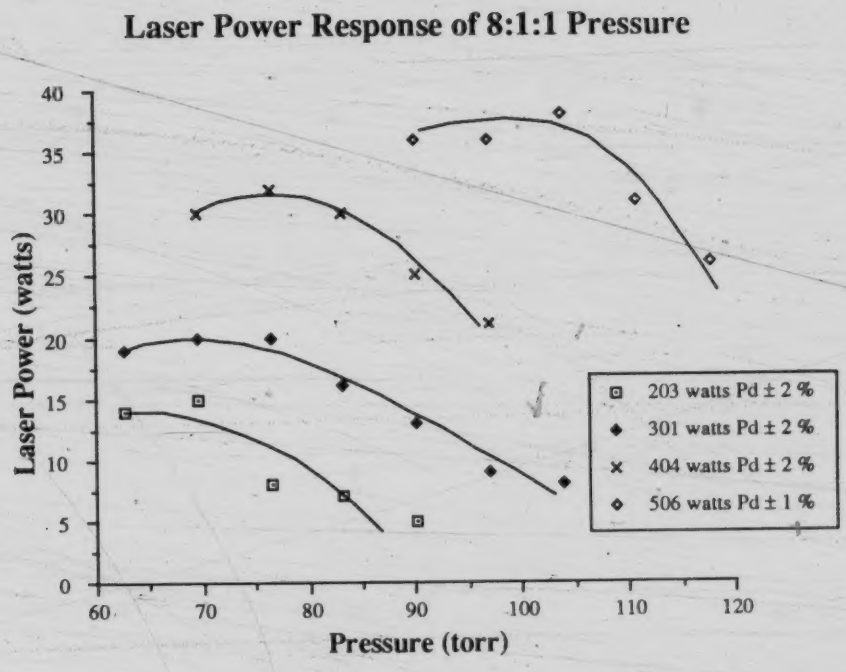

Figure 3.7 The change in laser power for variations in gas pressure for 8:1:1 ($He:CO_2:N_2$)

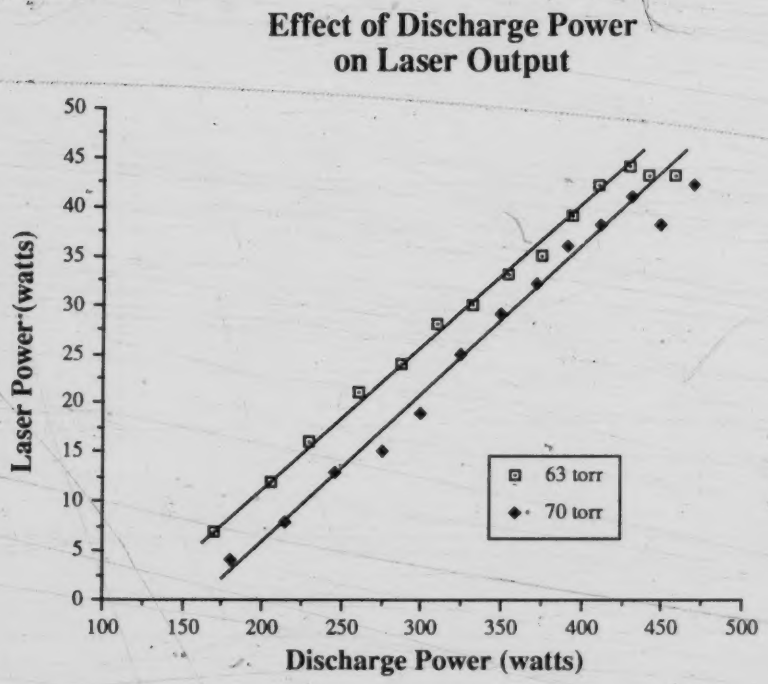

Figure 3.8 The change in laser power for 3:1:1 (He:CO_2:N_2) as the discharge power is varied. The two pressures that produced best power in the pressure experiment are used.

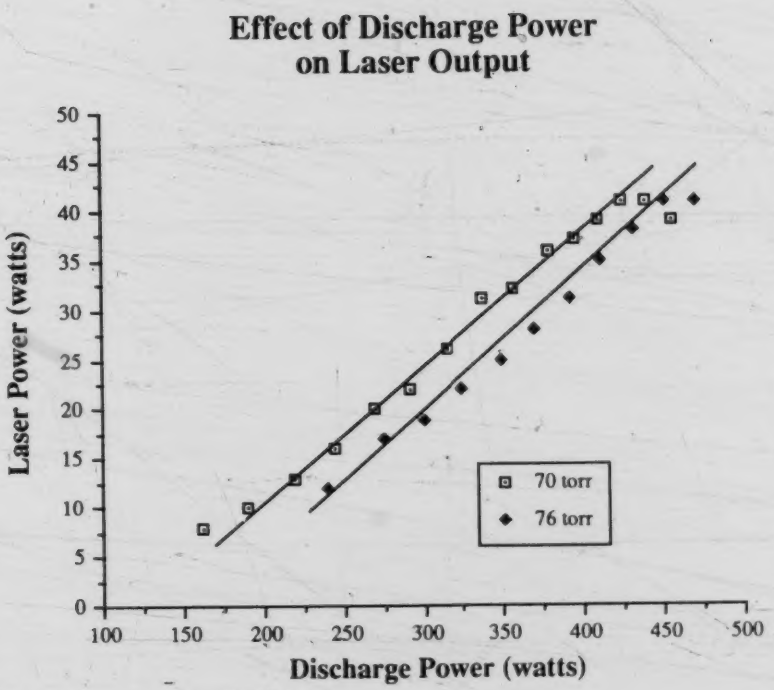

Figure 3.9 The change in laser power for 4:1:1 ($He:CO_2:N_2$) as the discharge power is varied. The two pressures that produced best power in the pressure experiment are used.

Figures 3.8 and 3.9 present the results of two experiments on the response of output power versus the discharge power. For this test the gas pressure was held constant along with the gas mixture, and the input RF drive swept across the range of interest. From these graphs, the laser power response is linear, but flattens abruptly at 425 W P_d. Typical discharge laser power plots roll off in power gradually, unlike these. The increasing power side of the curve is proportional to the excitation (RF drive), and the roll off is due to the increasing population of the lower laser level, from increased gas temperature caused by the additional discharge power. Output power using 4:1:1 ($He:CO_2:N_2$) was not significantly different from the 3:1:1 curves, but was shifted from 63 torr to 70 torr. Beyond 400 W P_d, the laser mode control was deteriorating, due to thermal loading, and the abrupt power fall off is attributed to this. Tests of the thermal loading will be discussed in the next section. With a more stable structure the laser could produce more power than has been demonstrated here.[37] The optical instabilities could, however, be sufficiently adding to a thermal power fall off such that optical stability improvements may not increase the power output.

For these gas mixtures over the ranges tested, 3:1:1 ($He:CO_2:N_2$) produced comparable, if not more, output power than 4:1:1 or 6:1:1, at any discharge power level. However, 4:1:1 ($He:CO_2:N_2$) did produce slightly more power, but at a higher pressure than 3:1:1, at 400 W P_d. Comparisons of the gas mixtures and pressures is made in figures 3.10 to 3.12, which contain the data from figures 3.4 to 3.7 replotted against constant discharge power. The displayed points have a range of ± 2.5 W and are typical for all laser power measurements of the 3/30 laser, these are due primarily to time varying thermal shifts in the optical system causing variations in optical power. At 500 W P_d all the mixtures except 8:1:1 produced 44 to 45 watts. These powers were produced at pressures increasing

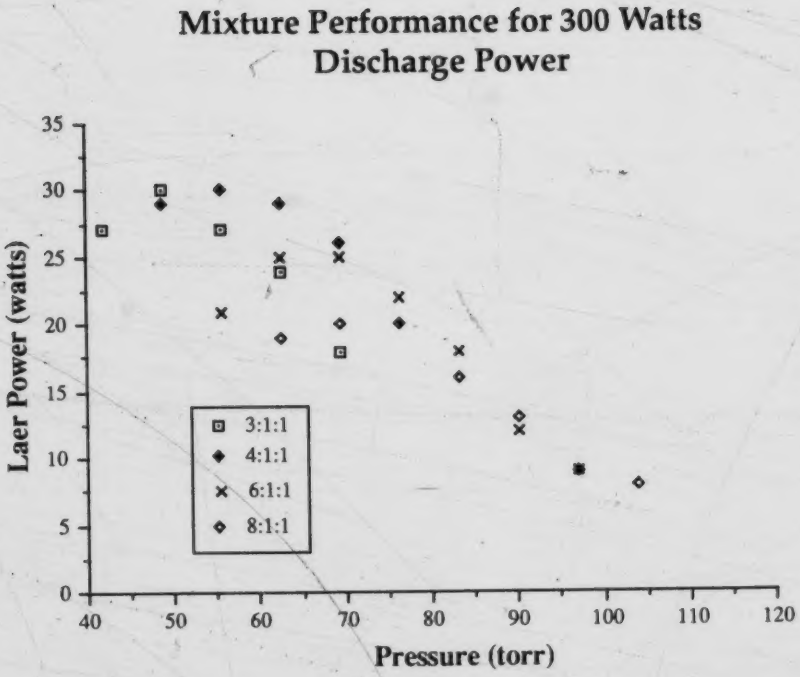

Figure 3.10 For constant discharge power, gas mixture and pressure are varied. Mixture ratio is ($He:CO_2:N_2$).

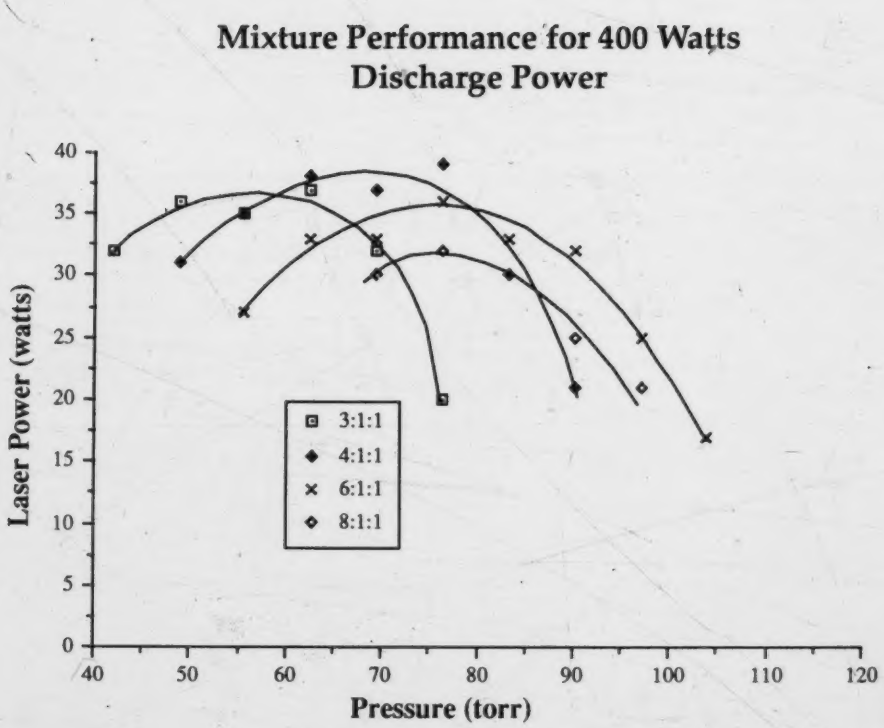

Figure 3.11 For constant discharge power, gas mixture and pressure are varied. Mixture ratio is ($He:CO_2:N_2$).

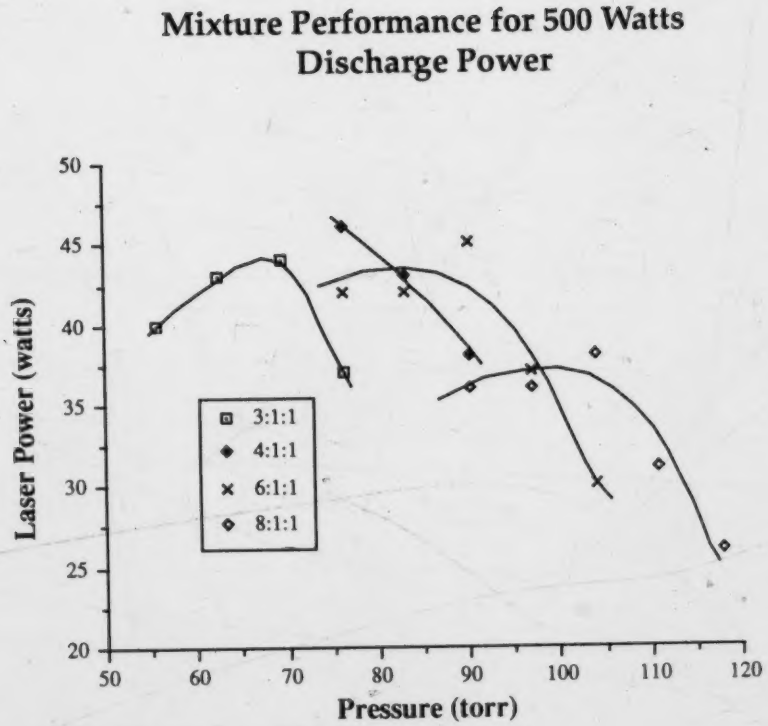

Figure 3.12 For constant discharge power, gas mixture and pressure are varied. Mixture ratio is ($He:CO_2:N_2$).

from 70 torr to 90 torr for 3:1:1 to 6:1:1 respectively. Taking into account the experimental errors, dilutions to 6:1:1 produce acceptable efficiencies of 9% at 500 W P_d and all could be used to produce a usable laser at these powers. The standardization of 3:1:1 for the remaining tests on this laser was done, as it acceptable efficiencies of 9% at 500 W P_d and all could be used to produce a usable laser at these powers. 3:1:1 was standardized on for the remaining tests on this laser, as it did not improve or degrade response significantly over the other gas mixtures. Additionally, it was available as a premixed gas which eliminated mixture related errors in the power measurements.

Since the gain of the laser medium is proportional to the relative density of CO_2 in the mixture, having to run at rich mixtures indicates a significant optical loss. Richer mixtures have peak power at lower pressures while leaner mixtures shift the maximum power to higher pressures, but lower its maximum value.[35] The 3/30 slab laser needs rich mixtures for optimal power output, which indicates the laser has too much optical loss for the gain available. Optical effects are considered in section 3.4.

For the RF energy to efficiently couple into the CO_2 molecules, an optimum electric field must be applied to the gas.[7] A convenient measure of this applied field is the electric field to pressure ratio, E/P. An optimum value of 7.5 V/cm–torr produces efficient excitation of a mixture of 3:2:1 ($He:N_2:CO_2$); this E/P value is used since a value for 3:1:1 ($He:CO_2:N_2$) was not available but the mixtures are close.[5] The gas under test was 3:1:1 ($He:CO_2:N_2$), which is a slightly richer mixture than 3:2:1 The optimum E/P tends to increase with the density of CO_2, therefore, the richer mixture should have a higher E/P ratio. From figure 3.13 it is seen that the measured E/P ratio exceeds this optimum value, except at the highest power and pressure reported (500 watts at 76 torr). During the

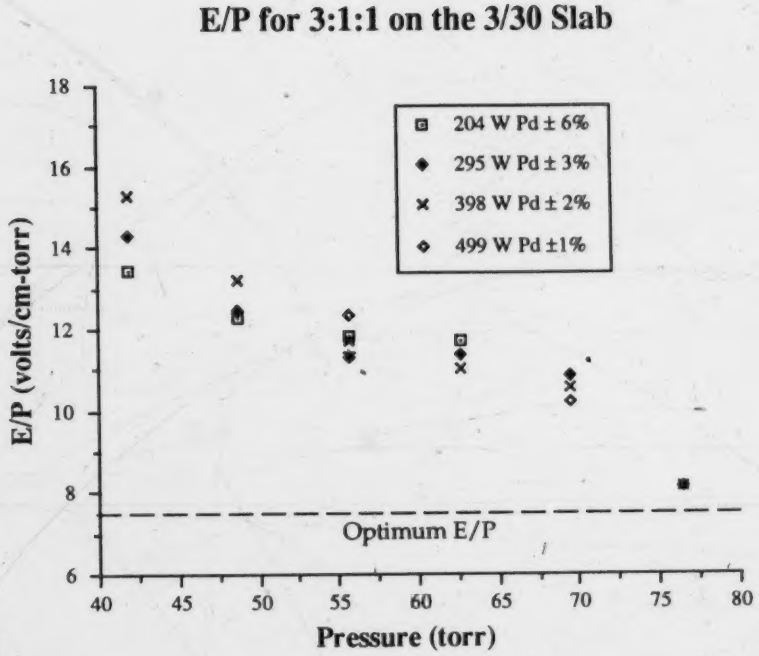

Figure 3.13 Electric field to pressure (E/P) measurement for the 3/30 slab laser. A gas mixture of 3:1:1(He:CO_2:N_2) is used. Optimum E/P is for 3:2:1(He:N_2:CO_2).

experiment the voltage probe loaded the electrical system, and a drop in laser power was apparent after the change in discharge power was taken into account. The voltage trend does indicate that at higher powers a better E/P could be achieved, resulting in greater excitation efficiency and laser output.

3.3 Thermal Measurements

The electrode temperature was measured to determine the laser running temperature, and assess its effect on the laser power. To accomplish this a thermistor was placed in a hole in the electrodes—both lower and upper. It was found that the lower (ground) electrode reached a maximum temperature of 25°C after 20 minutes at 500 W discharge power. The upper (hot) electrode reached a maximum temperature of 32°C under the same conditions.

This is consistent with the laser construction, since the electrically hot electrode is cooled through a 1 cm thick boron nitride insulator, and the ground electrode is cooled directly by the cooling plate in the bottom of the vacuum chamber. The electrodes are running warmer than desired—room temperature. With an inlet cooling temperature of 15°C, it is observed that the cooling effectiveness is poor. Carter et. al.[12] found that an increase in the wall temperature of 10°C produced a 20% decrease in power; therefore, approximately 8 W could be gained by cooling the electrodes to 20°C. Cooling does not fully account for the loss of output power at the measured discharge powers, but will have more effect at kilowatt power loadings in future lasers. Optimally, conducting heat out of the laser was given greater consideration in the 3/60 cm laser design discussed in chapter 4.

3.4 Optical Measurements

During gas characterization it was found that a rich mixture was optimal for the 3/30 laser, indicating that it could be optically lossy. Optical losses can arise from waveguide irregularities, mirror losses and from excessive output coupling. Temperature measurements show the laser is losing some power from gas heating, but not significant amounts. Consideration of the optical loss mechanisms is appropriate for the optimization of this laser, and future slab laser designs.

Waveguide irregularities, stemming from surface roughness, bends in the guide, and absorption losses have been dealt with in chapter 2. Having had the guide surfaces finished on the microsurface lathe and the short 30 cm length (minimizing bending loss), this guide would not contribute to excess optical system loss. Mirror losses can take three forms: absorption, diffraction and coupling. The mirrors used were gold on a copper substrate with a reflectivity at 10.6 μm of 99.4%.[38] Mirror absorption is not a significant factor in the optical path losses, based on this value. Diffraction and coupling losses[39] were dealt with in chapter 2, and since the resonator structure falls into one of the low loss categories it should not cause excessive losses if the mirrors are placed against the guide.

Gas breakdown to the mirrors was the limiting factor in placing the mirrors close to the waveguide. The mirror waveguide separation was 5 mm, which is double the typical separation used with CO_2 waveguide lasers. Mirror separation was decreased to 3 mm with the subsequent maximum power increasing from 44 W to 52 W at 525 W P_d, 10% efficiency. It is not possible to

move the mirrors closer to the guide as gas breakdown starts to occur from the plasma.

To measure the output power coupling it was necessary to analyze the beam profile. Wood burns and an electro–optic beam analyzer were used to determine the cross sectional beam profiles, and these profiles were used to assess the power coupling. The percentage output coupling was based on the assumption that the intracavity intensity was uniform. This assumption does lead to inaccuracies when compared to the intracavity profiles reported by Rensch[47] but is the best that can be made without intensity measurements. Figure 3.14 provides a schematic view of the electro–optic beam analysis system. Beam profiles were captured on wood in both the near and far field in addition to the beam analyzer. Burn marks are not sensitive to the absolute intensity but give a qualitative feel to the beam profile in three dimensions. The damage threshold for each wood target is different and the recorded beam profile will vary from measurement to measurement dependant on the total exposure time. The electro–optic beam analyzer provides absolute intensity information but only samples the beam in two perpendicular slices.

To make these beam measurements some modifications to the basic system shown in figure 3.14 were needed. Addition of a fan to blow particles away from the output coupling window was necessary to minimize the damage incurred to the window from particulate heating when making burns in wood. To obtain an accurate near field analysis it was necessary to reverse and flip the analyzer over to move the scanning element closer to the output window. This was needed since the scanning element is not centred in the analyzer and would place an additional 5 cm distance in the beam path before measurement. In the

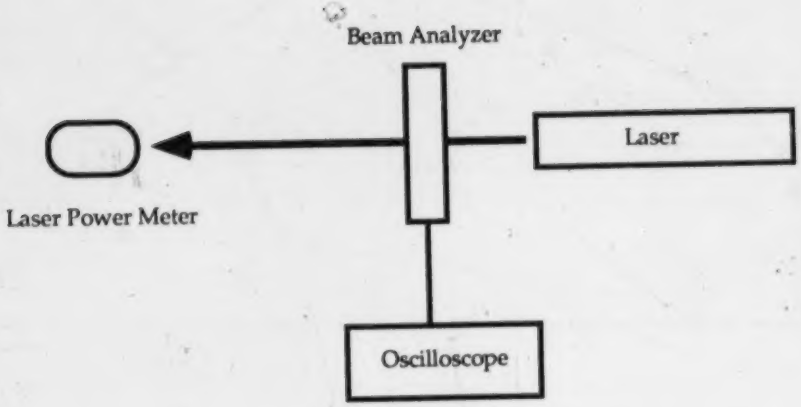

Figure 3.14 Experimental Beam Analysis Setup

reversed position the analyzer would not measure the vertical axis, waveguide mode, due to a malfunction of the detector only in this orientation.

Near field burns indicate that the beam was 4 to 5 mm wide, approximately double the expected 2 mm, and having twice the geometric output coupling than is desired. In these burns the beam profile was flared and ragged on the waveguide edge. The mirror spacing to the guide edge was 2 mm which put the outside 2 mm of the beam beyond the waveguide causing the ragged edge. Figure 2.8 shows the off axis resonator and the mirror gap *d*. Variation of the mirror gap from 2 mm to 7 mm indicated that there was no change in beam width, and no laser power variation. The mirrors have been standardized to 4 mm gaps as this provides the clearance needed to propagate a 4 to 5 mm beam confined to the channel area, while limiting interaction with the waveguide supports.

Figure 3.15 displays the near field unstable resonator beam profile, and figure 3.16 shows the far–field profile with the output mirror gap at 7 mm. For figure 3.15, the near field, the front mirror edge is on the left side of the trace while in figure 3.16 the front mirror is on the right. The "notch" on the extreme left side of the traces is a scanner artifact.

Little change in beam shape was recorded with variation of the gap *d*, and the beam cross–section with a 7 mm gap is representative of those observed. The zero order approximation of a uniform near field beam profile is far from reasonable for this resonator when the actual near field profile is observed. A nonuniform profile was the result of diffraction dominating the output The near field beam width is 6 mm taken at the beam's zero power points (from figure 3.15) while from geometric theory it should be 2 mm. Burn records indicated a 4 to 5 mm beam (exposure dependant). The discrepancy between burn marks and

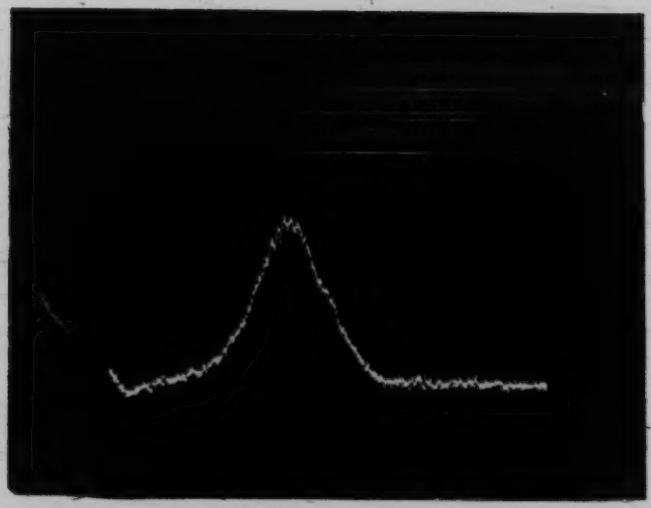

Figure 3.15 Unstable Mode, Near Field 3/30 Laser
1.5 mm per Division Horizontal

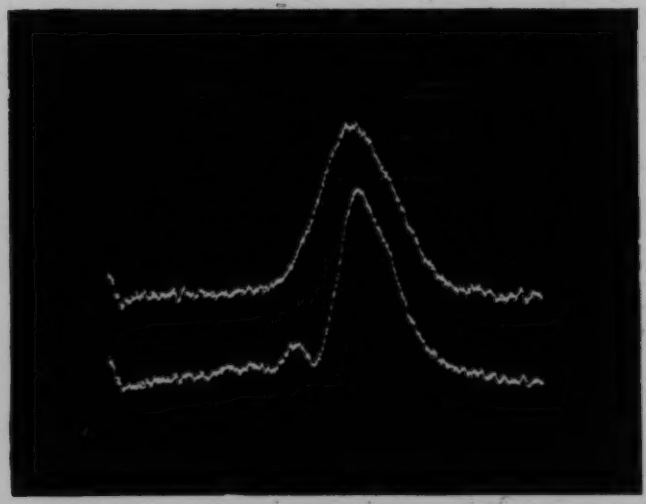

Figure 3.16 Far Field, 80 cm, 3/30 Slab Laser
Stable Mode is Top Trace
Unstable Mode is Bottom Trace
3 mm per Division Horizontal

the beam analyzer is caused by the damage threshold of the wood target causing a mark to form only the after a critical level of energy has been delivered.

In an attempt to reduce the geometrical power coupling a 3.2% coupling (18.6 m and –18 m) mirror set was constructed using 1100 aluminum (the standard mirrors of gold on copper were too expensive to fabricate at the time). The added optical loss from the 98.7% reflective aluminum[38] would lower the maximum power but not affect the beam shape. No difference in beam width was seen. However, this mirror set should have produced half the coupling of the 6.7% (9.6 m and –9 m) set, but with the thermal instabilities caused by the higher optical loss of aluminum at 10.6 μm, the effect of the mirrors was indeterminate. Flat aluminum mirrors were also tried with similar results to the 18 m mirrors. Output power was down by half from the 9 m gold optics with both aluminum mirror sets. Optics of 9 m radii, 18 m radii, and flats created the same near field beam width. With the nonuniform beam profile it is not possible to estimate the output coupling since it is possible that the intracavity profile is irregular as well.[28] It is not understood why the mirror curvature has no effect on the laser operation.

3.5 Power Scaling and the 1/30 Slab Laser

Earlier work with a 1 cm wide slab laser showed that it was capable of producing 27 watts (not optimized). If linear power scaling holds for the 3 cm wide discharge, with equivalent extraction efficiency, an 81 watt laser is possible. Since this output power was not observed with the 3/30 laser, it was necessary to measure the per unit power from the discharge. This per unit basis would determine if scaling was working when compared to the 1/30 slab laser. To test the power width scaling, a power per unit width test was conducted comparing the power from the 1/30 cm and the 3/30 cm lasers on a per unit basis.

The 1/30 cm laser was run to determine the best power obtainable. Commercial dielectric plano–plano optics were used for the 1/30 laser resonator. This produced a single mode in the narrow dimension, but did not limit the beam in the wide dimension to a single mode. Figure 3.17 shows the power output of the laser at the optimal conditions of 6.5:1:1 ($He:CO_2:N_2$) at 132 torr. These conditions optimized the power output. The discharge power was not increased above 400 W since the laser became optically unstable and produced unrepeatable results. To compare the 3 cm discharge, the 1/30 laser was removed from the vacuum housing and the 3 cm channel installed. The 1/30 optical system was used for the 3/30 unit but a 1 cm wide aperture was introduced into the optical cavity. This system sampled a 1 cm strip out of the 3 cm discharge for comparison to the 1/30 laser. The optimal 1/30 gas mixture and pressure was used for the 3/30 laser test.

For a per cm power loading similar to the 1 cm channel the 3 cm channel produced similar power output, but at 12% efficiency instead of 9%. Using the entire 3 cm width with similar power loading would produce 90 W of laser power.[40] Under the same gas and power conditions the 3/30 laser, with the unstable resonator, produces less power when using 6.5:1:1 ($He:CO_2:N_2$) than using 3:1:1. Under optimal conditions for the unstable optics, the 3/30 laser operates much as the 1 cm laser does. Figure 3.18 compares the optimized extracted power from the 1 and 3 cm lasers. Under the respective best conditions, the lasers compare in operational efficiency. Since the 3/30 slab laser has the predicted per unit power, the extraction efficiency of the unstable resonator must be lower than the plane–plane resonator to account for the lower net power output.

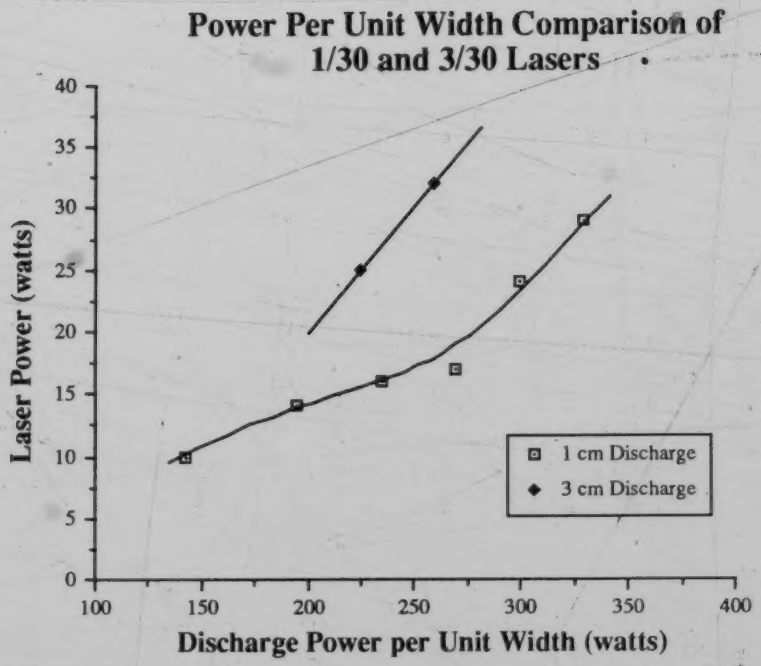

Figure 3.17 Comparison of the per unit width power production of the 1 and 3 cm discharges. A 3 cm discharge is used with a 1 cm apperture and stable plane–plane optics. A gas mixture of 6.5:1:1 (He:CO_2:N_2) at 132 torr is used (optimal for the 1/30 laser).

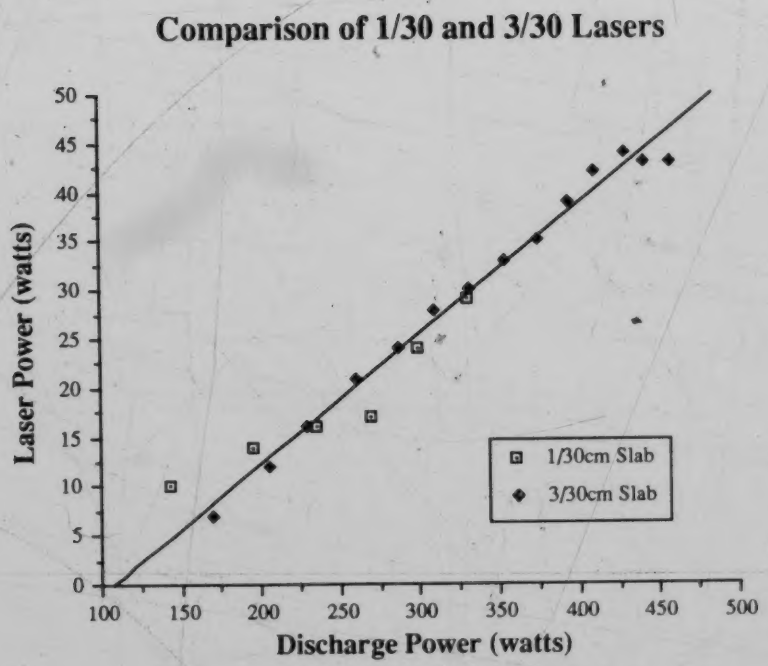

Figure 3.18 A comparison of the 1/30 and 3/30 lasers under optimal conditions. 1/30: 132 torr, 6.5:1:1 ($He:CO_2:N_2$). 3/30: 70 torr, 3:1:1 ($He:CO_2:N_2$).

3.6 Conclusion

The 3/30 laser has been shown to produce 52 watts at best optimization. Thermal instabilities in the optical system limit further consistent gains from this laser until more stable optical mounts are constructed. Gas optimization in both mixture and pressure was completed. The results show that 3:1:1 (He: CO_2: N_2) at 63 torr produces the most power. From the trends in gas characterization it is not clear whether these gas conditions will be optimal at higher discharge power loadings. Temperature measurements indicate that the laser is operating too hot for best power output, but this is not the limiting factor. Beam profile measurements have shown that geometric coupling designs do not create a beam with the desired coupling properties. The unstable resonator is responsible for the lower power extraction per unit volume than the stable resonator. It appears that power extraction is diffraction dominated and dependant on the resonator geometry rather than the optics.

Chapter 4: 5/30 and 3/60 Slab Laser Optimization

This chapter focuses on the experiments made to improve the original 3/30 slab laser to achieve a 100 W output. Modifications have taken several forms: length and width scaling, optical resonator modifications, and cooling improvements. The 5/30 cm and 3/60 cm slab lasers were used for these tests. Width and length scaling were used to increase the laser power in order to produce the desired 100 W. A 100 W laser was produced using the 3/60 slab. Resonator modifications were made to assess output coupling on laser performance, with the unexpected result that flat mirrors produced more power than the confocal sets. Cooling at kilowatt power loadings continued to be a problem which forced the introduction of a novel internal cooling scheme.

4.1 5/30 Slab Laser

Width scaling was implemented with the 5/30 cm slab laser. It was a retrofit of the 3/30 vacuum housing with modifications for a 5 cm wide channel and wider mirrors. Basic gas characterization was conducted, but little additional power production beyond the 3/30 laser was obtained.

Optimization of a laser for power is a matter of balancing the laser gain against the system losses. Once the losses are overcome, further gain increases go to power output. With proportionately greater losses, the gain must be increased to maintain the same output power. Therefore, to increase the power the active width was enlarged to 5 cm. This width was the maximum that could fit in the existing vacuum chamber and still leave space for the voltage balancing inductors. Using this electrode, the power would be multiplied by $^5/_3$ if linear width scaling held for this discharge based on the preceding lasers.

Scaling similarity relations given by Abrams and Bridges[40] hold for molecular lasers if the gas temperature and electron temperature are held constant. The electron temperature requirement keeps a constant per unit area power level in the discharge. It is necessary to maintain a constant gas temperature to keep the lower laser level at the same population state in order to have the same per unit gain. More efficient cooling is necessary to maintain the constant gas temperature at increased power loading. The cooling was not changed, therefore a higher gas temperature was expected, reducing the increase in power. Laser power should have scaled to approximately 75 W, not taking into account the thermal effects. Experiments did not indicate appreciable enhancements in power (figure 4.1) over the 3/30 slab, with 56 W being the maximum found. This test was conducted with 9 m optics at 6.3% geometric coupling under similar gas mixtures and pressures as the 3/30 laser.

Figures 4.2 and 4.3 display the effect of pressure on the laser power for the 5/30. A pressure of 63 torr produced the most power. Abramski,[42] and Jackson[2] at D. R. Hall's lab in the United Kingdom have done work on area scaling of slab discharges, and have found that the optimum pressure falls from the high used in square waveguide discharges to a lower stable value for slab discharges. They feel this is consistent with a shift to two wall dominated cooling from the four wall case. This is consistent with the findings of this experiment. The optimum gas conditions were much like the 3/30 in both mixture and pressure while the shapes of the response curves are also similar to those of the 3/30. Lean gas mixtures yielded less power in all cases. This was more pronounced than the 3/30, but optical stability was similar to that laser.

The 5/30 laser ran at poor efficiencies of 5% to 8% (figure 4.4). This may be caused by a poor voltage balance, but is unlikely since the end to end balance

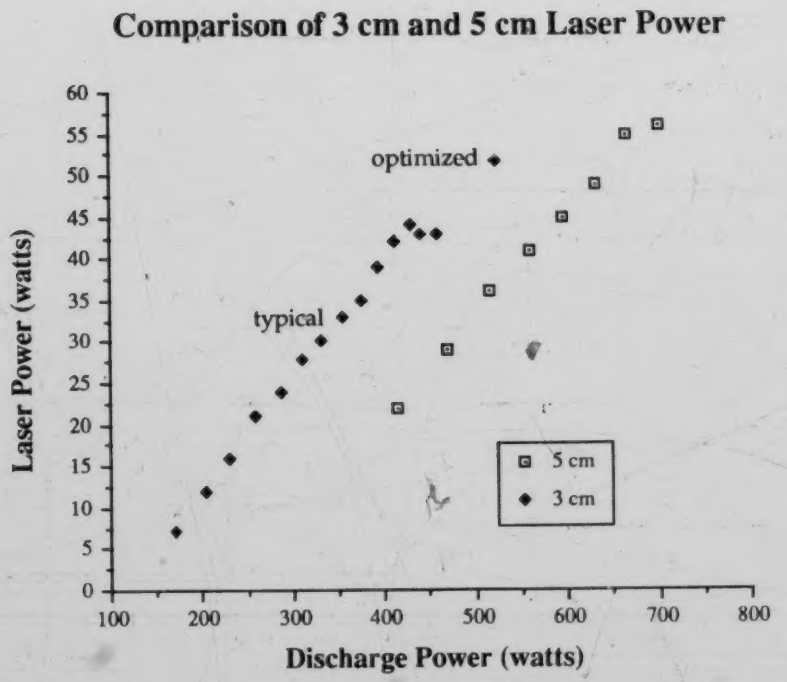

Figure 4.1 A comparison plot of the best power produced from the 3/30 and 5/30 lasers. Gas conditions for both lasers: 3:1:1 (He:CO_2:N_2) at 63 torr.

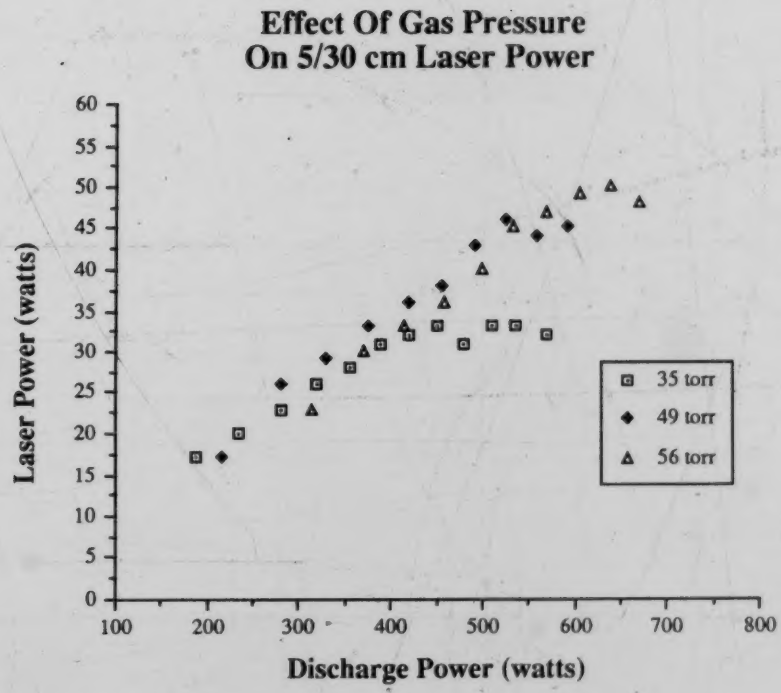

Figure 4.2 The change in laser power for 3:1:1 ($He:CO_2:N_2$) as the discharge power is varied.

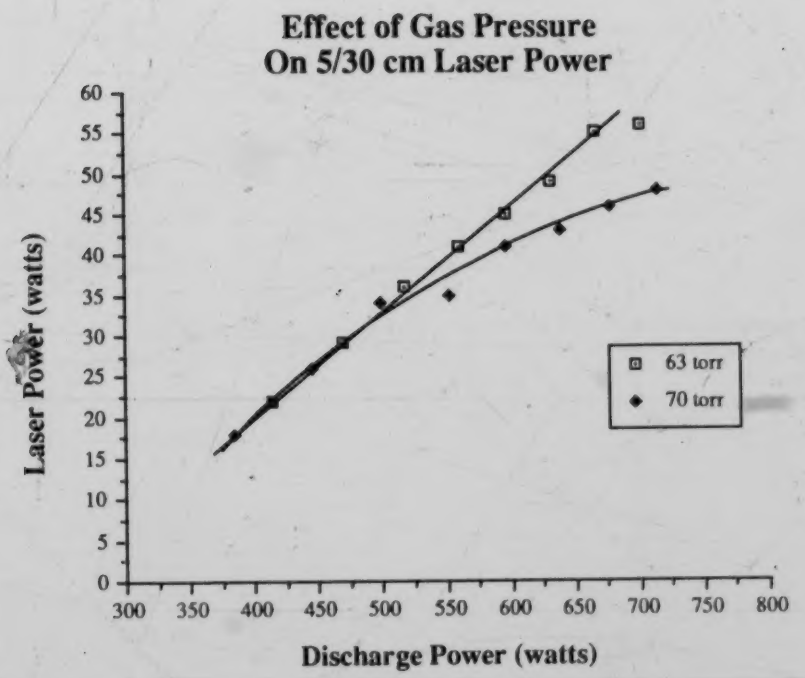

Figure 4.3 The change in laser power for 3:1:1 (He:CO_2:N_2) as the discharge power is varied.

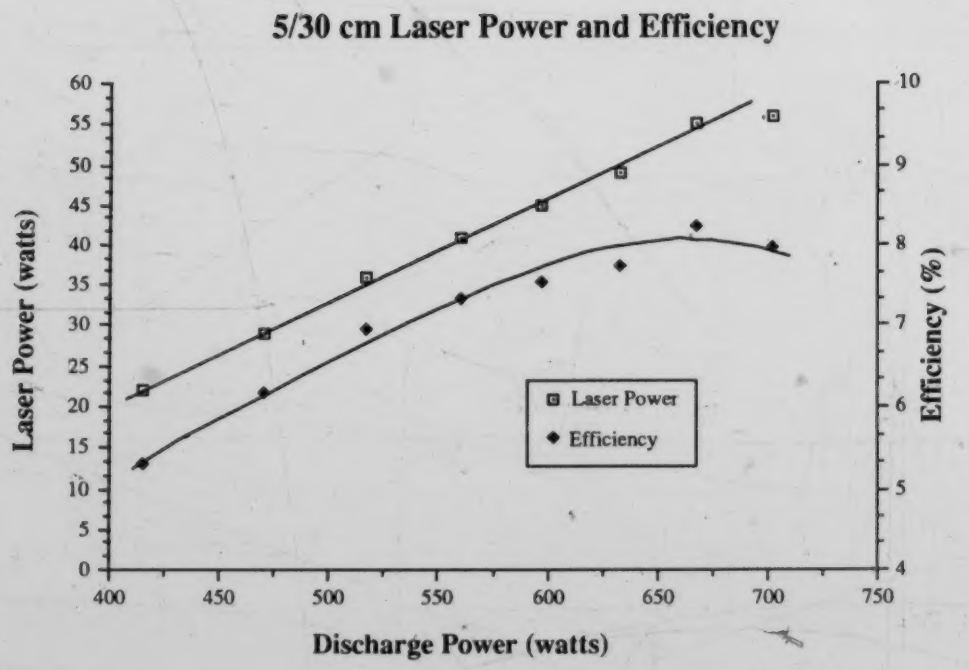

Figure 4.4 The optimized efficiency and laser power for the 5/30 slab. The gas mix is 3:1:1 ($He:CO_2:N_2$) at 63 torr. Efficiency is calculated as the ratio of laser power over net discharge power.

was better than 5% for the dischargeless case. During voltage balancing, no discharge is maintained, leading to inaccuracies in the final balance because the plasma acts as an unconsidered lossy element, with a dischargeless tuning. Voltage balancing inductors are located inside the vacuum housing making it impossible to tune with the laser running.

The voltage balance across the wide dimension of the discharge was difficult to sustain, as indicated by plasma brightness variations. Variation of the plasma intensity across the width of the discharge was noted, which established regions of gain nonuniformities, lowering power output. Due to space limitations in the laser housing, it was not possible to use inductive voltage balancing on both sides of the channel.

No temperature measurements were taken, but from measurements made on the 3/30 slab, temperatures at fall off on the order of 30°C to 40°C could be present. Having gas temperatures this high will reduce the output 20% to 30%. Combined influences such as these can account for the loss in expected power increase, as observed. Limitations in the RF power amplifier and gas cooling were further causes of lowered actual power extraction. With improved cooling and a thermally symmetric optical system, laser power may reach the 100 W goal.

4.2 3/60 Slab Laser Design

Since the 5/30 laser was not capable of 100 W output, more changes to the slab design were needed. With the 3/60 laser, a clean break was made from the previous designs to reach the 100 W goal. Thermal, optical, and gas parameters were considered for this laser to overcome noted shortcomings in previous designs. Hard-sealed long lifetime laser construction was also considered, with the intent of building a laser with a 1000 hour lifetime. Completion of a prototype

3/60 slab laser and the hard–sealed counterpart was made, but due to failure of the lifetime analysis vacuum system, the hard–sealed slab was not tested.

The 3/60 optical system was improved for stability, and consequen ly provided a good platform for further resonator experiments. Directly cooled electrodes were introduced in the 3/60 which improved the thermal response of the laser, but not sufficiently for continuous use with kilowatt power loading. Recommendations are made for the next generation of slab lasers with emphasis on sealed–off operation and long lifetimes.

Losses identified with prior tests have centered about two main areas: thermal and optical. Thermal instabilities limited work at high powers to produce the requisite 100 W output. To remove the instability a thermally symmetric optical system was designed, and is shown in figure 4.5. All major mechanical components are made of aluminum using machinable ceramic as spacers between them. To ensure thermal stability, the vacuum envelope was constructed of 0.065" thick INVAR sheet and seam welded to form a tube.

Channel cooling was made by pressing copper tubing into machined slots in the back of the electrodes. This provided the best compromise as water cannot be in contact with aluminum without severe corrosion occurring. The corrosion process is further enhanced by the applied electric fields during laser operation. Liquid corrosion inhibitor was not practical for use in semi–portable dental/surgical equipment without the introduction of recirculating pumps and the associated equipment. Surface passivation of aluminum parts is difficult to implement, as the facilities to coat the 60 cm long channels are not readily available.

To cool the electrodes directly the water must pass through the vacuum chamber wall and into the electrode. For short experiments the feed–through

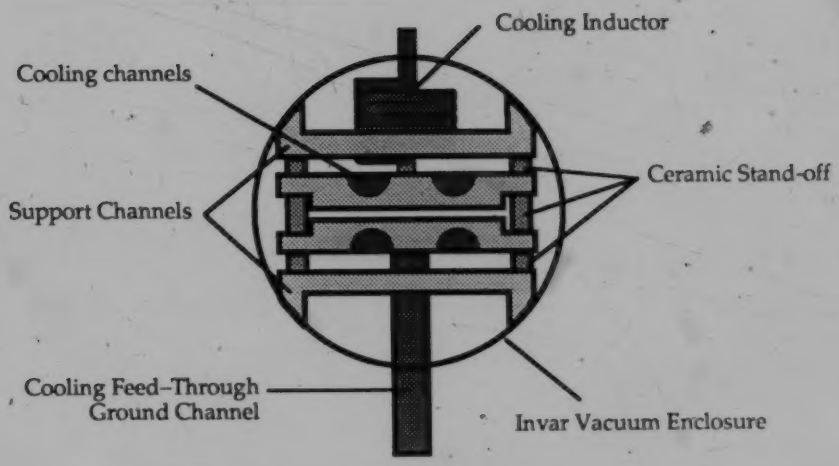

Figure 4.5 3/60 Slab Laser Cross–Section

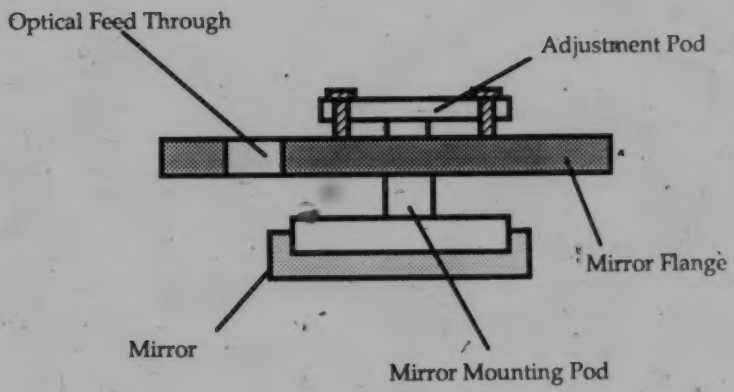

Figure 4.6 3/60 Mirror Mount: Top View Cross–Section

material is not critical and could be chosen as any insulating material. To maintain good vacuum properties over extended periods, the feed–through must be a low reactive metal, such as stainless steel. For the ground electrode, a metal tube creates a better ground connection to the case and improves the electrode mechanical strength However, a direct metallic connection cannot be made to the electrically hot electrode or it will short to ground (the case). To circumvent the hot electrode short, some form of feed–through was needed.

Two types of feed–through were examined. The first involved a ceramic feed–through to isolate the cooling tubing, and the second method isolates the tube by inductive decoupling. Ceramic feed–throughs were not used on the experimental version of the 3/60 slab for reasons of mechanical strength. They were incorporated into the second 3/60 version after inductive decoupling proved too restrictive on water flow. However, on the first 3/60 laser inductive decoupling was used, and is shown in figure 4.5. One end of the inductor connects to the hot electrode, while the other goes through with the metal vacuum housing wall. Water is passed through the tubing used to form the inductor and into the press fit tubes in the electrode back. This method proved reliable and sufficient for the initial work but let the electrodes become too hot for optimal use.

The cooling inductors became part of the voltage balancing network and act in parallel to the channel to channel coils used. To maintain sufficient inductance with the voltage balancing coil, the "cooling" inductance must be kept large, compared to the balancing inductor. A prerequisite to meeting this requirement was using $1/8$ in. copper tubing, which kept the inductance large in a small enough space to fit into the laser. This $1/8$ in. copper tubing introduces a significant pressure loss, but can be overcome if sufficient inlet pressure is

available. Increased pressure loss reduced coolant flow, offsetting some expected temperature decrease from direct channel cooling.

Voltage balancing inductors were placed on the channel ends, inside the vacuum housing, for the experimental laser. For long lifetime operation this is not acceptable due to the reactive nature of copper with free oxygen formed by the discharge, and the oxides that copper produces. Oxidization of copper removes O_2 from the laser gas, furthering the disassociation of CO_2 and decreasing the laser operational lifetime. In future slab lasers, balancing inductors will be outside the enclosure, but the resistance inherent in the INVAR vacuum chamber complicates the balancing, since the voltage drop over the housing surface depends on applied power. Thermal stability and cooling capacity are improved with these design changes, leaving optical stability and losses to be covered.

Using a stable, symmetrical mirror mount, position instabilities in the mirror have been decreased. Figure 4.6 shows a cross–section of the front mount. The mirror is attached to a pod which allows a three point adjustment to shift the mirror. Mirror pod movement is coupled through the vacuum housing by a 0.010 in. thick diaphragm which deflects under force from the positioning screws, transmiting the deflection to the mirror pod mounted on it. This has proved to be a much more stable mount than used on the 3/30 and 5/30 laser, but because of increased intra–cavity flux in the 3/60, the mounts were still thermally reactive.

Design and construction of the matching network comprised the final section of the 3/60 laser. It was necessary to construct a variable matching network to deliver 1000 W to the laser in a reliable manner. Several types of matching circuits were considered, with a Pi–network formed from discrete L C elements being the most flexible for the driven load.

4.3 Matching Networks

There was a need for an adjustable impedance matching circuit for the operation of the laser at 100 W output levels. A kilowatt of RF power must be delivered to the laser for this power to be achieved. The network used for previous slab lasers was a $\lambda/4$ transformer. This is a compact system at 72.5 MHz, with cable lengths approximately 60 cm long. It is also robust and introduces small losses to the power delivery system, but only a few select impedances can be formed with the commercial cable available. To obtain small VSWRs, the circuit must be adjustable while the laser is in operation, so that any parasitic impedances can be nulled, and a good match formed. Circuits that have been considered are the Pi, L, T, and autotransformer, shown in figure 4.7.

Sinclair[5] has examined L– and T–networks with the most successful being the circuit of figure 4.7a. On using this T–network with the 3/60 slab, voltage breakdown across the series capacitor occurred proving it not rugged enough for this laser. The autotransformer of figure 4.7d was initially introduced by Moghbeli[17] and has found wide use in conventional waveguide lasers in the Medical Laser Lab at this university. However, the slab laser has a discharge resistance less than 50 Ω, making the transformer difficult to tune while maintaining a resonant circuit with the laser channel.

Hybrid networks using cable transformations and lumped elements have been in use since the earliest work on RF waveguide lasers was reported. Griffith[43] used a capacitive L–network with a tuned cable section to transform the laser impedance to 50Ω. This has led to the design of a combination lumped circuit and cable section for use with the 3/60. Ruling out most of the viable lumped networks left only the Pi– and L–networks for consideration.

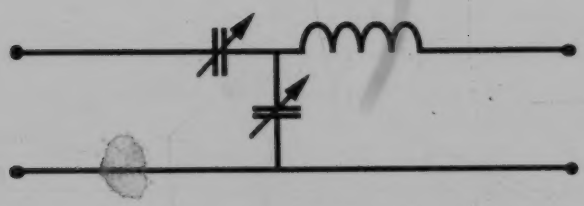

Figure 4.7a T–Network

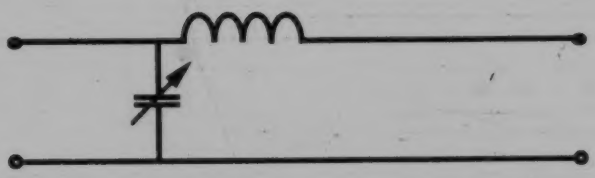

Figure 4.7b L–Network

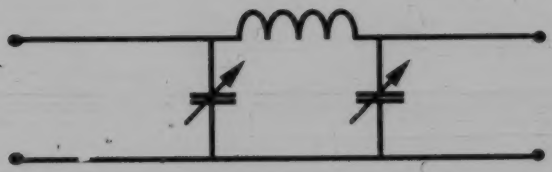

Figure 4.7c Pi–Network

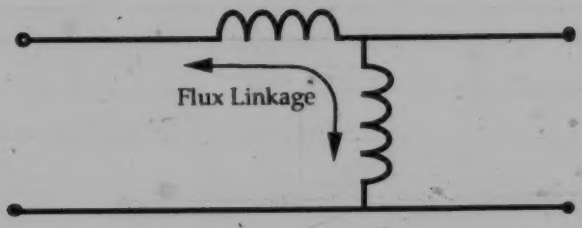

Figure 4.7d Auto-transformer

The 28Ω $\lambda/4$ transformer was used in combination with these networks to minimize the impedance range for the lumped components to match across. Doing so lowered the circulating current while reducing network losses and increased the operational ruggedness. Operational variations in the discharge impedance were most effectively reduced by the pi–network which gave the broadest matching range. The usable power range was from 500 W to 1000 W with the lower limit set by the laser impedance moving outside the tuneable range of the circuit. As the network was designed to power the laser at the highest output possible, it did not match well to the impedance seen at 500 W and less. A 1 kW RF power meter module was the highest available which limited the metered operation to 1 kW. To commercialize the laser, a network that will have a very broad match will be required.

4.4 3/60 Experimental Results

The 3/60 slab laser was used as a test bench for a variety of experiments. Effects of gas mixture and pressure were investigated, and tests varying the geometrical coupling were conducted. This was the first slab laser to operate under sealed–off conditions, and gas optimization was conducted to achieve a 100 watt laser. Optical and thermal stability and thermal overload of the gas became apparent with continuing tests.

The initial experiments were made using optics with 5% geometrical coupling. They were designed and fabricated the same way as all the mirrors used prior to this set. Curvatures of –23.4 m and 24.6 m were machined in oxygen free copper using the microsurface lathe,[44] with a coating of zinc selenide applied for surface stability over a coating of gold. This combination was thought to

produce a mirror of lowest loss and still have good abrasion resistance, while slowing the effects of the gas plasma on the gold.

Flowing gas was used for the first experiments, using this new laser to provide an operational starting point. The standard experimental equipment, as used in previous laser tests, was used for these experiments. Gas mixture was varied to find an optimum ratio, but as with the 3/30 slab laser 3:1:1 ($He:CO_2:N_2$) was found to produce the most power. Using flowing gas conditions, an experiment to find the best operational pressure was conducted. The premixed gas, 3:1:1 ($He:CO_2:N_2$), was used and maximum laser power obtained for a given pressure was recorded. A P_d of 1 kW was held for this maximum power experiment. Figure 4.8 illustrates the results obtained, and shows that at 50 torr the most power was produced. The optimum pressure and power obtained with flowing gas was 99 W of laser power at 1 kW P_d with 50 torr, 9.9% efficiency. This power output was easy to obtain under flowing conditions, and no attempt was made to further optimize the laser with flowing gas. The laser power meter could measure 100 W full scale, and the RF power meter was limited to 1 kW. Primarily these tests were conducted to find a general operational base from which to compare the sealed off experiments.

The reason for developing the 3/60 laser was to overcome the deficiencies identified with the 3/30 laser. Preliminary beam measurements conducted on this laser indicated that the near field beam was approximately 7 mm wide. Similar results were found on the 3/30 laser. A detailed look at the geometric coupling properties of a slab unstable resonator were called for. Geometric couplings of 5% and 10% were used in both the positive and negative branches of the stability plane.

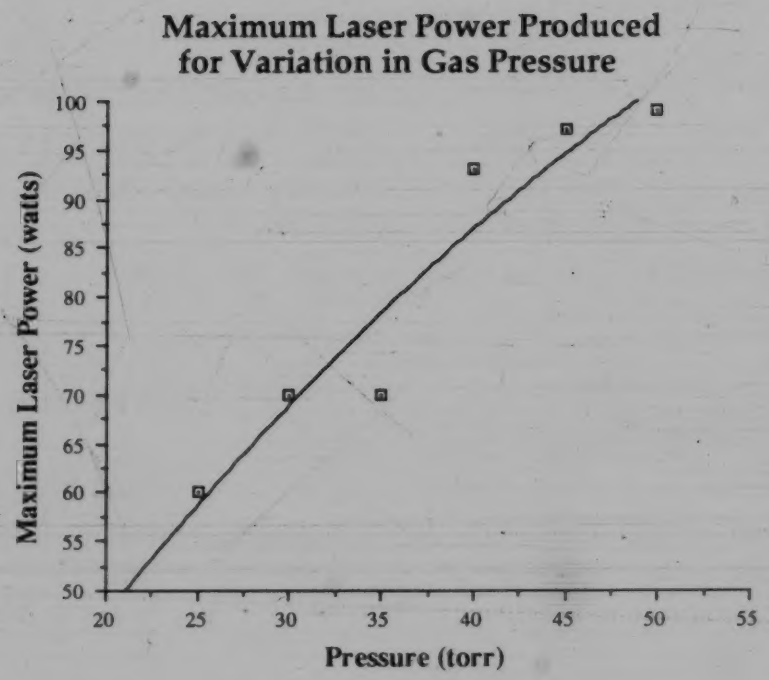

Figure 4.8 The maximum laser power produced by the 3/60 laser using 3:1:1 ($He:CO_2:N_2$) as the pressure was varied. Flowing gas was used.

It was noted during 3/30 testing that the output mirror had to be moved to increase the gap to the edge of the active region. This was done to maintain waveguiding at the outside edge of the beam, and to improve the beam profile. The gap formed by the output mirror edge and the outside edge of the gain region is defined as d, as shown in figure 2.8. Gaps of 4 mm and 7 mm were used, although to geometrically fill the gain region, a d of 1.5 mm and 3 mm should be used for geometric couplings of 5% and 10%.

Using these parameters, burns were made in plexiglass to show the beam structure. Figure 4.9 represents the experimental equipment, and figure 4.10 is a picture of the 3/60 laser experimental work bench. Plexiglass was chosen over an electronic analyzer since it gave much better resolution, and left a three dimensional impression in the plastic from which it was easier to see the overall beam shape. From these modal profiles, a series of photographs have been taken for presentation purposes. A representative set showing the basic features is included in this section, with table 4.1 listing the maximum stable and unstable dimensions in both the near and far field. The maximum extent of the burn is taken, because the e^{-1} points are difficult to measure in the plexiglass with any certainty.

The negative branch unstable resonators produced only 1 W to 3 W and were extremely optically unstable. No mode could be maintained for more than a few seconds. This behaviour can be explained by the intra–cavity focal spot that is produced during operation by the optical resonator. Focusing of the intra–cavity beam will cause localized heating such that the active region could be sufficiently perturbed to distort the beam, and stop effective laser action.

Positive branch resonators were operated with a constant discharge power of 700 W. All curved mirror sets produced approximately 65 ± 3 W using 50 torr

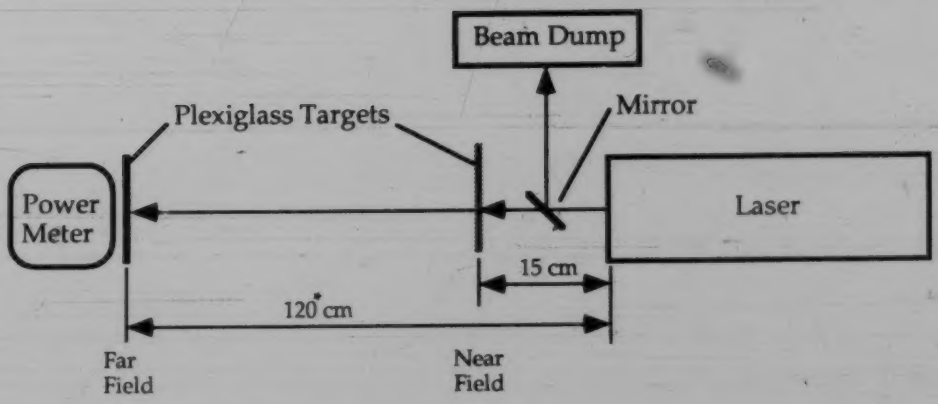

Figure 4.9 "Plexiglass" Mode Profile Experiment

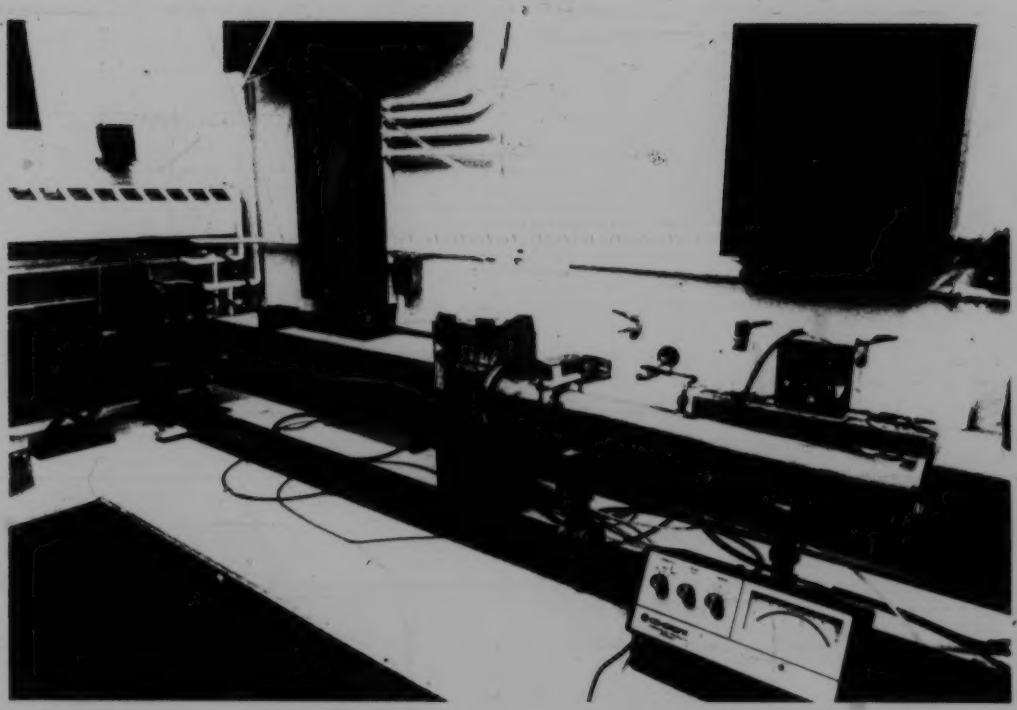

Figure 4.10 3/60 Slab Laser and Experiment Area

Table 4.1
Optical Resonator Geometrical Coupling Experiment
Positive Branch Unstable and Flats
Width of Melt Zone

Near Field (mm)		Far Field (mm)			
Stable	Unstable	Stable	Unstable	Coupling (%)	Gap
2.8	7.5	13.2	12.6	5	4
2.8	9.1	12.9	10.7	5	7
2.9	9.5	15.7*	12.7	10	4
3.1	9.4	12.6	13.7	10	7
4.6	8.0	17.9	12.5	Al Flat*	4
3.5	8.5	14.0	12.0	ENAL	4
3.5	9.7	(8.5	9.2)†	ENAL	5

* Multi-mode operation — a single mode could not be maintained

† Far field burn made at 80 cm

of 3:1:1 ($He:CO_2:N_2$). The flat aluminum mirrors produced 10 W more power, unlike the enhanced aluminum (low loss multilayer dielectric coating) which operated at lower temperatures and with more stability.

Near field burn widths in the waveguide resonator dimension, normal to the channel, are comparable to a EH_{11} gaussian beam. The average measured maximum beam width was 3 mm, with 2.25 mm channel spacing and 2.03 mm at the e^{-1} points for a EH_{11} mode. Pictures of the near field show a triangular intensity variation with fresnel diffraction ripples on top, caused by the mirror edge (figures 4.11 through 4.13). The near field unstable dimension, parallel to the channel, is typically 8 to 9 mm. No significant difference was found from 5%, 10% or flat aluminum mirrors. Figure 4.12 shows a small lobe (below the main burn pattern) in the stable dimension which was typical of multimode operation and was seen in other burns. The fresnel ripples from the ENAL (ENhanced ALuminum) mirrors were more numerous and better defined (figures 4.15 and 4.16). It is not known why this was the case, but it was consistent throughout the experiment. These findings would suggest that the discharge is significant in this resonator design, at least at the small geometric output couplings used. It also indicates that the resonator departs considerably from the geometric case.

Seigman[29] notes that for the lowest order unstable modes the output beam tends to pull in its "wings" which lowers the output coupling from the geometric case. This predicts a narrower beam than a geometrical design. The results presented here show the contrary. In all cases the beam was two to four times the geometrical width. High order unstable modes have greater diffractive losses and greater beam spread. Increased beam spread does fit the observed data, and greater output coupling fits with the need to use rich gas mixtures. However, excessive mirror heating was seen (see the section on ENAL mirrors and mirror

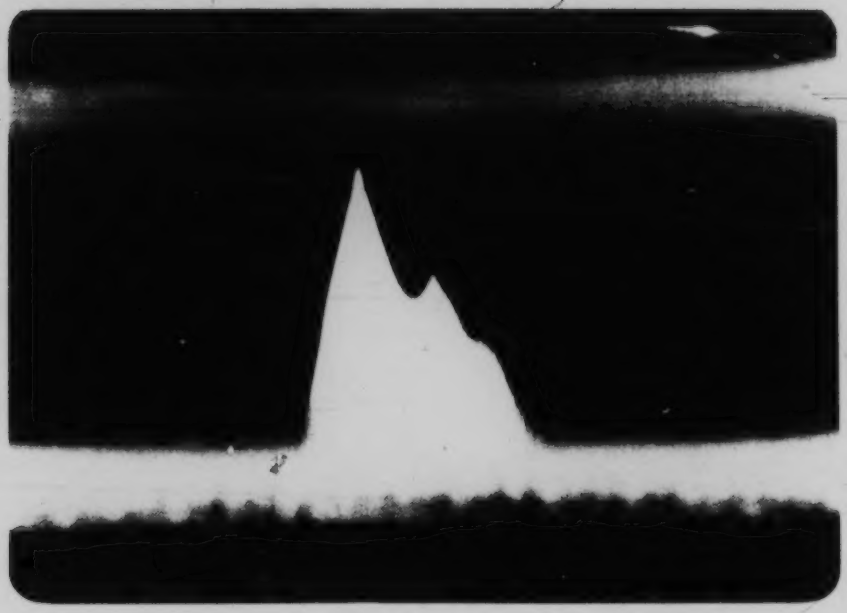

Figure 4.11 5% Coupling Near Field, Side View

Figure 4.12 5% Coupling Near Field, Top View

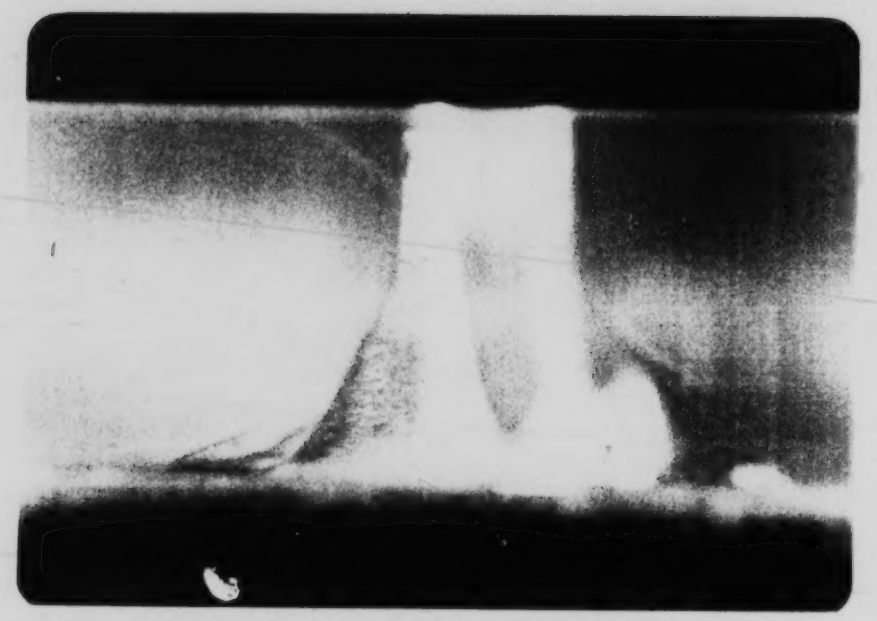

Figure 4.13 5% Coupling Near Field, End View

Figure 4.14 5% Coupling Far Field, Top View

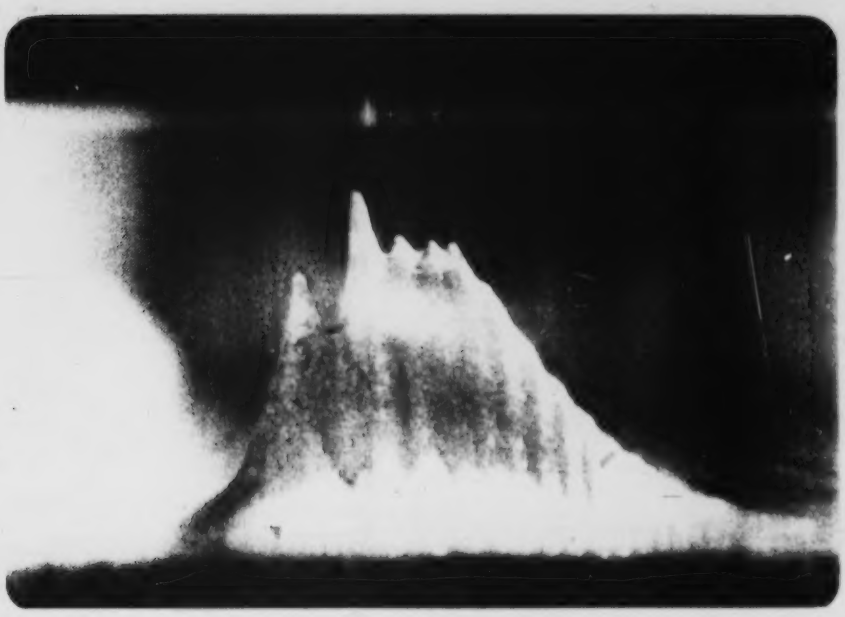

Figure 4.15 ENAL Near Field, Side View

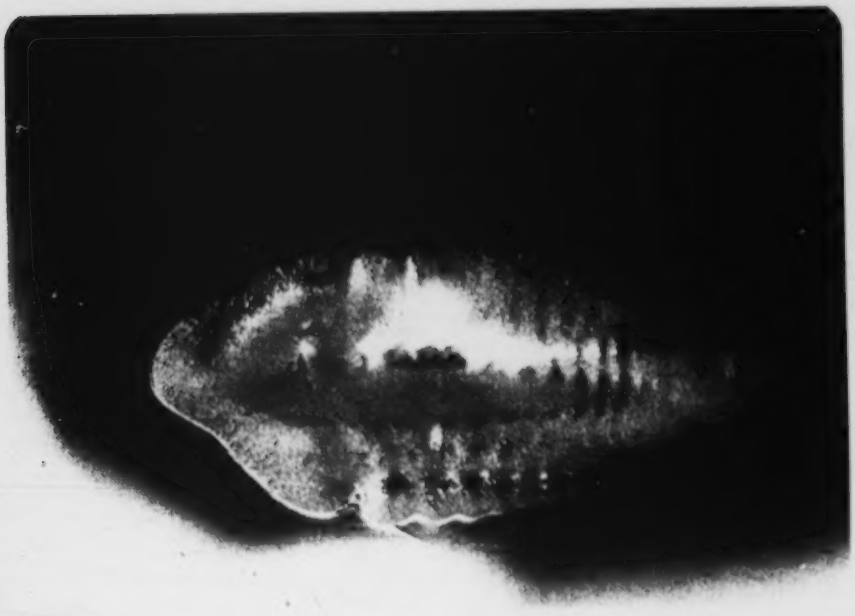

Figure 4.16 ENAL Near Field, Top View

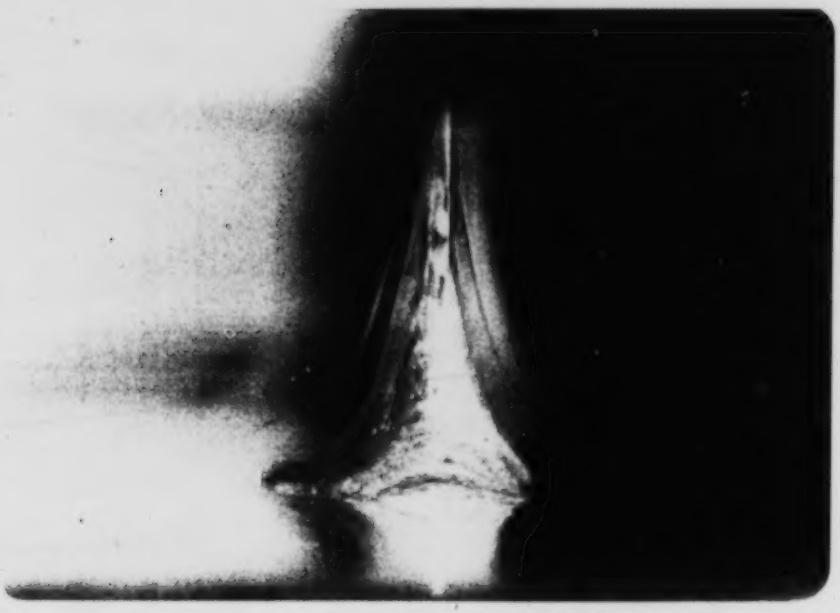

Figure 4.17 ENAL Near Field, End View

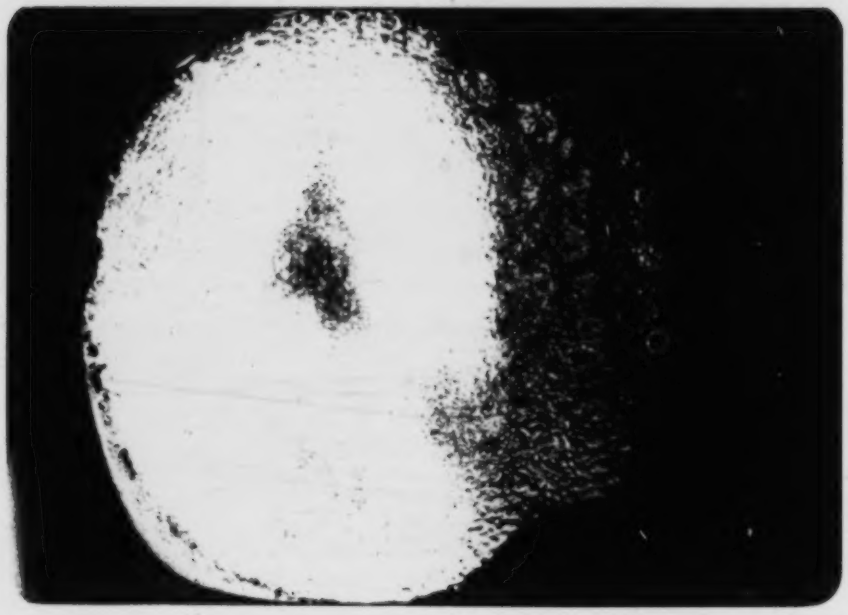

Figure 4.18 ENAL Far Field, Top View

temperature) which would indicate the resonator is under coupled or the mirrors have high losses. The experiments to date have not shown conclusively what is the cause of the beam spreading, or the greater than expected optical losses. Having the unstable modes propagating through the waveguide could be the cause of the deviations from that reported in the literature.

The far field beam shape is gaussian in the stable direction, but shows a $\sin(x)/x$ like trail of secondary lobes going away from the mirror edge, and a gaussian like intensity fall–off towards the mirror. EH_{11} beam propagation gives a waveguide beam width at the e^{-1} points of 10.5 mm (120 cm) or 7.15 mm (80 cm), which agrees with the experimental values of 12 to 13 mm and 8.5 mm for maximum beam dimension. Some multimode operation, in the waveguide dimension, is seen and could cause the added beam spreading. The main lobe of the unstable beam is 6 mm across while the main lobe after propagation of a rectangular beam from the laser output aperture is 4 mm wide. Comparing the primary lobe of the unstable mode to that caused by fraunhofer diffraction of a rectangular beam indicates that the unstable mode is likely coherent. This measure of coherence is very limited, but does provide an estimate.

The flat mirrors produced the same beam shape as the confocal sets, with the exception that the low loss ENAL mirrors operated at lower temperatures and were more stable than the plain aluminum. This is attributable to the greater absorption of 10.6 μm radiation for plain aluminum versus the multilayer dielectric coating on the enhanced mirror. Based on these findings, it was decided to use flat aluminum mirrors and then, as they became available, the ENAL mirrors for sealed off work with the 3/60 slab laser.

For the sealed–off experiments the laser was pumped down to less than 1 torr and back filled with laser mix to the desired pressure. Figure 4.23 is a

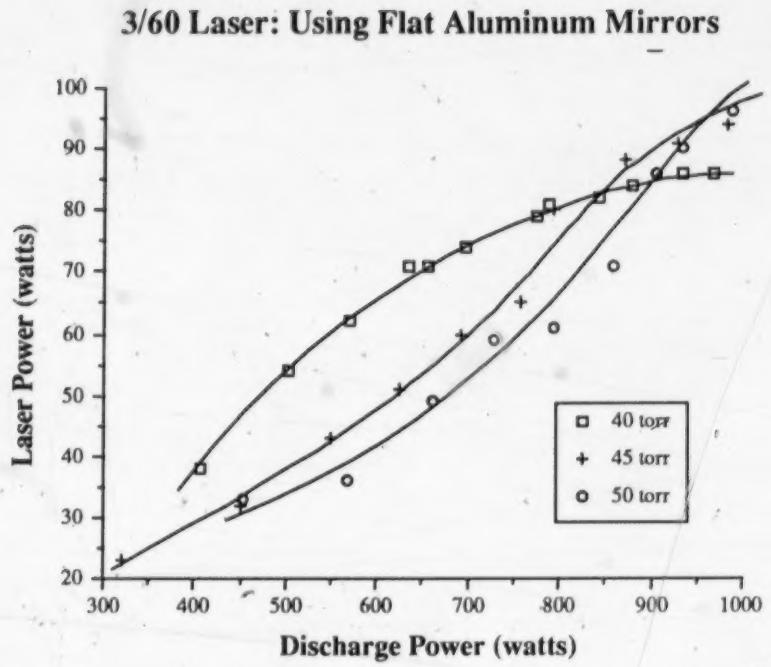

Figure 4.19 The change in laser power for 3:1:1 ($He:CO_2:N_2$) as the discharge power was varied. Static gas conditions, no flow.

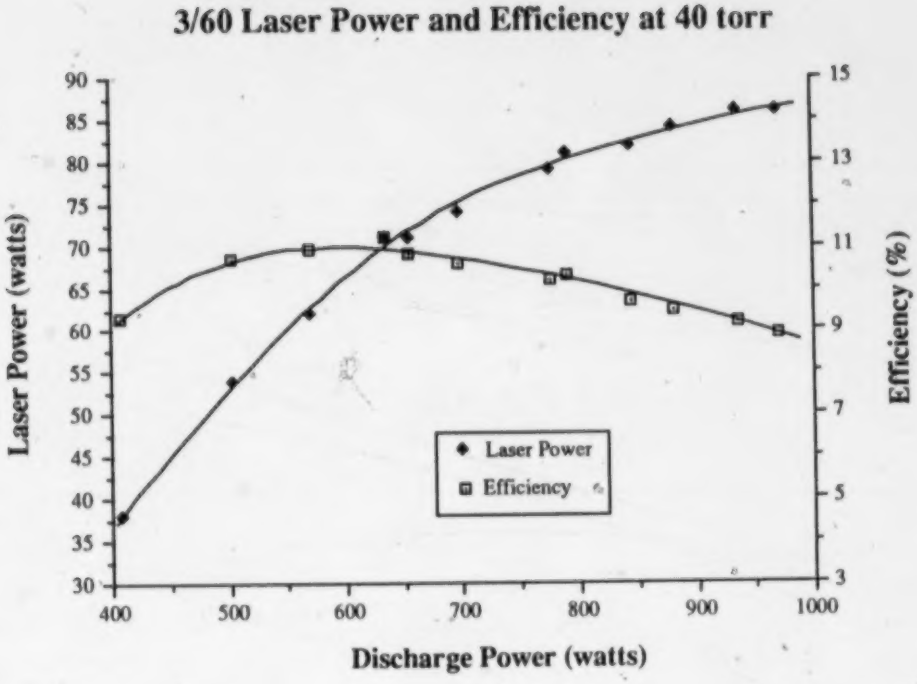

Figure 4.20 The efficiency and laser power for the 3/60 slab. The gas mix is 3:1:1 (He:CO_2:N_2) at 40 torr. Efficiency is calculated as the ratio of laser power over net discharge power.

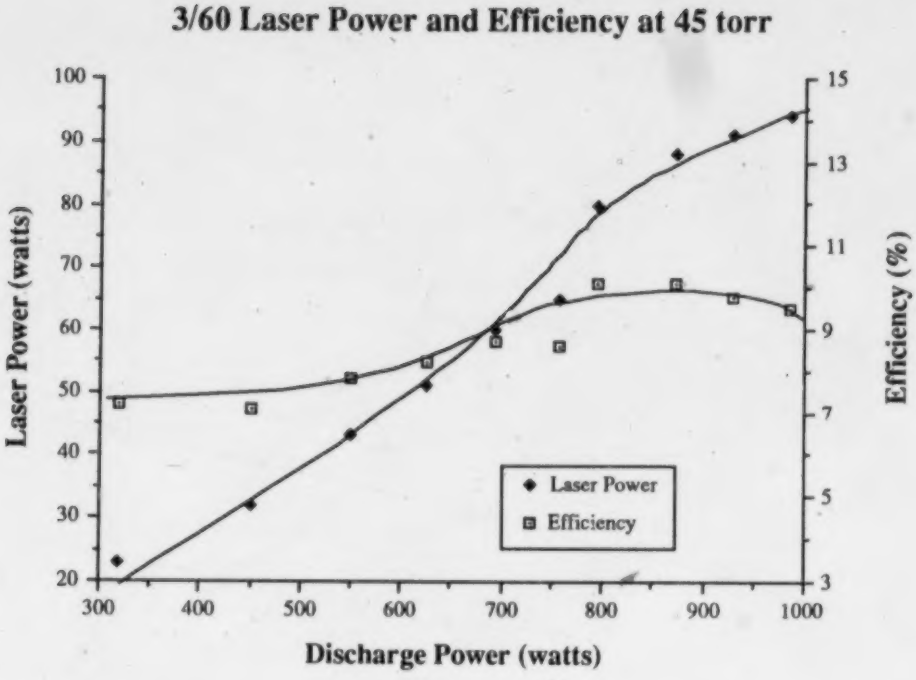

Figure 4.21 The efficiency and laser power for the 3/60 slab. The gas mix is 3:1:1 ($He:CO_2:N_2$) at 45 torr. Efficiency is calculated as the ratio of laser power over net discharge power.

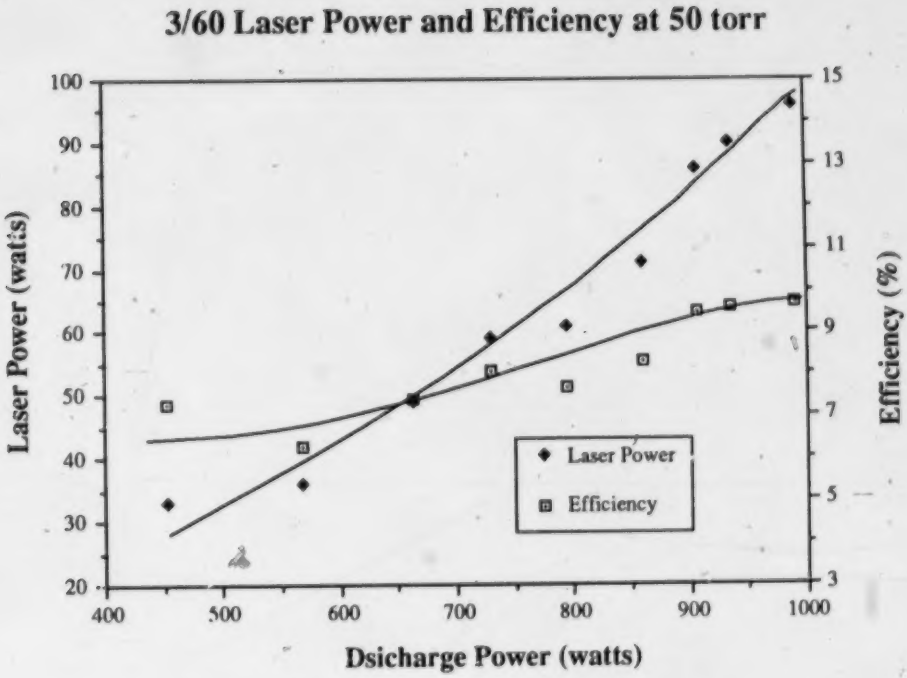

Figure 4.22 The efficiency and laser power for the 3/60 slab. The gas mix is 3:1:1 (He:CO_2:N_2) at 50 torr. Efficiency is calculated as the ratio of laser power over net discharge power.

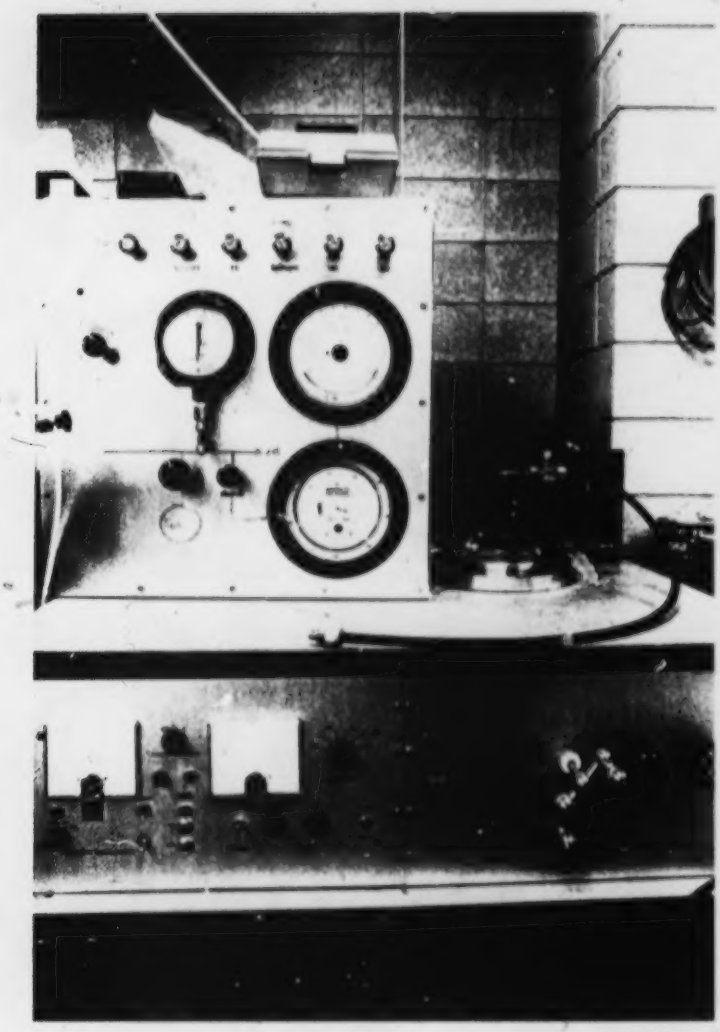

Figure 4.23 Vacuum System for Sealed Off Experiments

photograph of the vacuum system used for these experiments. The laser was soft sealed with rubber o-rings and no special cleaning was taken to optimize the sealed laser lifetime. Using this procedure enabled the laser to operate for approximately an hour before needing to be refilled, which was sufficient for the testing undertaken.

The gas mix used was 3:1:1 ($He:CO_2:N_2$) as no leaner mix had worked as well on this laser. Gas pressures were varied to find the optimum. Figure 4.19 shows the results of this experiment. Power output increased with gas pressure to 50 torr, but it was not possible to strike the discharge at 55 torr and above. The maximum laser power obtained was 97 W using 50 torr. The 40 torr power curve shows saturation in power output, but the 50 torr curve has not begun to level out. It should be possible, if sufficient RF drive were available, to produce more than 100 W of output.

Efficiency using 40 torr peaked at 11% with 550 W in the discharge (figure 4.20). At higher pressures the maximum efficiency moved up in power to 800 W at 45 torr, and to 1000 W at 50 torr (figures 4.21 and 4.22). However, at 50 torr the maximum was reached at the top end of the RF power supply, therefore the maximum could be at a higher discharge power. The maximum power typically is produced past the point of best efficiency. This is consistent with work done on earlier CO_2 waveguide lases,[5,7] which found that the maximum power output occurred past the peak laser efficiency.

During these tests the mirrors became extremely hot. Indium shims used to increase the mirror heat sinking melted slightly, under prolonged operation. (The melting point of indium is 157°C.) To reduce the optical losses in the mirrors, a multilayer dielectric coating was placed over the base 1100 aluminum flats. These enhanced mirrors functioned similarly to the plain aluminum mirrors

Table 4.2
Operating Temperatures for 3/60 Slab Laser

Laser Off

	Water (°C)	Channel (°C)
Hot Electrode	12.8	18.8
Gnd Electrode	12.5	19.3

1 K Watt Discharge

	Water (°C)	Channel (°C)
Hot Electrode	19.1	50.6
Gnd Electrode	15.0	34.7

(see the section on mode profiles) except they operated at lower temperature. No further power or efficiency increases were seen, and, except for a more stable optical system, the ENAL mirrors functioned the same as the aluminum flats.

Laser power was seen to drop off after the first few seconds of operation. Using the ENAL mirrors, start up output power was 97 W with 800 W discharge power, falling to 84 W laser power within 10 to 20 seconds. This is a sign that the gas is becoming too hot and the gain was dropping.[45,28] Laser power thermal effects were not noticeable until the more stable ENAL mirrors were used. Measurements taken on the input/output cooling water, and electrode temperatures show that the laser is reaching 51°C with 1 kW of discharge power. Table 4.2 summarizes the findings. The key result is that the water temperature increases only 6°C while the powered (hot) electrode increases by 32°C.

The large temperature differential across the cooling water to the hot electrode could be the result of three effects. Deposits could have accumulated in the cooling channels, but the laser had not been in operation for more than 6 months, making this unlikely. Too great a pressure differential could exist across the cooling system feed–through inductors. They are made out of $^1/_8$ in. copper tubing and the ΔP at typical flow rates is 15 psi. Two coils and the associated plumbing produced a flow of 900 ml/min with the tap fully open—typically 40 psi. Having low cooling flow rates would increase the water output temperature, but the majority of the temperature drop is across the channel to water interface. This seems the most likely bottle-neck to lowering the running temperature of the electrodes.

A further iteration on the 3/60 laser was completed, but not tested under the scope of this work. It increased the number of press fit cooling tubes in the electrodes from 2 to 4 and replaced the decoupling inductors with an insulated

feedthrough. This should improve the cooling and improve the power performance. (This laser has not been operated above 500 W P_d to date.)

4.5 Conclusion

Width and length scaling of the discharge was accomplished and by using the 3/60 laser 100 W was produced. Unfortunately, the 5/30 laser did not produce significantly more power than the 3/30 laser did. This was attributed to thermal and optical instabilities. Thermal and optical stability problems were addressed in the 3/60 laser, but not sufficiently to produce a commercial product. Output beam profiles were recorded for this laser and consequently the confocal resonator was replaced with a plane–plane system. The output was consistently two to four times that predicted by geometrical theory. This was considered a result of modal interaction with the waveguide structure and its influences on the active region, but conclusive data was not taken. Power extraction was done by edge diffraction past solid metallic mirrors, using the same optical system as the confocal resonator. With gas optimization and improvements in the optical system, a maximum power of 97 watts was produced using the 3/60 cm slab laser.

Chapter 5: Conclusion

The slab laser has met the goals of supplying 100 W of laser power while maintaining the advantages found in all metal lasers. Although some design deficiencies are indicated by the experimental work described, the overall usefulness of this RF waveguide geometry has been demonstrated. Many questions have been answered over the course of this work, but further questions have come to light.

Three major classes of experiments were conducted on the slab laser. Discharge scaling, gas optimization, and optical resonator experiments formed the major areas. Discharge dimensions of 3 cm by 30 cm, 5 cm by 30 cm, and 3 cm by 60 cm were used in scaling experiments. These lasers were then used in gas and optical experiments, to optimize the laser power. It was found that scaling the discharge length was necessary to overcome optical losses and create enough gain to produce a 100 W laser. However, if lower power lasers are called for, the smaller gain volumes can provide reasonable output powers of 30 to 70 W. As such, these lasers should be developed further with more emphasis on the specific capabilities they possess.

Gas optimization was performed by examining the effect of pressure and mixture on the lasers. The most extensive tests were conducted with the 3/30 slab laser, and indicated that the laser structure was losing more power than designed for, and consequently was not performing optimally. Similar results were found on the 5/30 and 3/60 lasers.

All experiments point to excessive loss from the optical resonator and optical instabilities. Gas mixtures optimized at 3:1:1 ($He:N_2:CO_2$) indicated that a

high gain discharge is necessary to overcome losses. No direct gain measurements were performed on these lasers. Of all the possible loss mechanisms, over–coupling or excessive power extraction from the resonator are the major factors. The deviation from predicted geometrical coupling indicates an overly diffracted beam, but the underlying cause has not been definitively determined. Interaction of the unstable resonator modes with the waveguide through nonlinear discharge effects could be the cause, but insufficient data is present to know conclusively.

The published literature carries few examples of low magnification high aspect ratio confocal unstable resonators. This type of strip resonator has not been applied to CO_2 lasers before its use in this project. Clearly, from the questions raised over power extraction and the lack of pertinent literature more work is called for in this area. Simulation of the optical system would be beneficial, but because of the low magnification new techniques would have to be developed.[29]

Optical stability could be one of the major factors in commercializing the slab laser. The course of this work has not demonstrated long term optical stability. That combined with the difficulties in cooling could limit the maximum power attainable. It seems certain that a product capable of 100 to 200 watts is possible from the slab, but further extrapolations above this power level are at best speculation.

A 100 watt laser was shown to be possible from the slab concept, but the lasers constructed have left room for definite improvements.

Reference

1 L. Lachambre, J. Macfarlane, G. Otis and P. Lavigne, "A Transversely RF-Excited CO_2 Waveguide Laser," DREV Internal Report M-2446/78, Mar., 1978.

2 E. Jackson, H. J. Baker, and D. R. Hall, "A CO_2 Large Area Discharge Laser Using an Unstable–waveguide Hybrid Resonator," preprint from *Appl. Res. Lett.*, Dec., 1988.

3 L. A. Newman, R. A. Hart, J. T. Kennedy, A. J. Cantor, and A. J. DeMaria, "High Power Coupled CO_2 Waveguide Laser Array," *Appl. Phys. Lett.*, Vol. 48, no. 25, 1986, pp 1701-1703.

4 L. A. Newman, and R. A. Hart, "Recent R&D Advances in Sealed–off CO_2 Lasers," *Laser Focus/Electro–optics*, June, 1987, pp 80–91.

5 R. L. Sinclair, "Radio Frequency Excited CO_2 Gas Waveguide Lasers," M. Sc. Thesis, University of Alberta, Fall 1983.

6 B. A. McArthur, "Sealed Radio Frequency-excited Carbon Dioxide Waveguide Lasers," M.Sc. Thesis, University of Alberta, Fall 1986.

7 P. Vidaud, D. He, and D. R. Hall, "High Efficiency RF Excited CO_2 Laser," *Optics Comm.*, Vol. 56, no. 3, 1985, pp 185-190.

8 D. R. Hall, E. K. Gorton, and R. M. Jenkins, "10 μm Propagation Losses in Hollow Dielectric Waveguides," *J. Appl. Phys.*, Vol. 48, no. 3, 1977, pp 1212-1216.

9 D. He, D. R. Hall, "Longitudinal Voltage Distribution in Transverse RF Discharge Waveguide Lasers," *J. Appl. Phys.*, Vol. 54, no. 8, 1983, pp 4367-4373.

10 Mr. M. Paulson—a member of the Surgical Laser Lab at the University of Alberta has developed a 40 watt waveguide laser constructed with a homogeneous guide.

11 Hughes Lasers are constructed with an all–ceramic guide.

12 G. M. Carter, and S. Marcus, "A High-power CO_2 Waveguide Laser," *Appl. Phys. Lett.*, Vol. 35, no. 2, 1979, pp 129-130.

13 J. G. Xin, and D. R. Hall, "Multipass Coaxial Radiofrequency Discharge CO_2 Laser," *Optics Comm.*, Vol. 58, no. 6, 1986, pp 420-422.

14 M. W. Sasnett, "Kilowatt–class CO_2 Lasers Meet Present And Future Industrial Needs," *Laser Focus/Electro–optics*, March, 1988, pp 48–67.

15 W. B. Veldkamp, J. R. Leger, and G. J. Swanson, "Coherent Summation of Laser Beams Using Binary Phase Gratings," *Optics Lett.*, Vol. 11, no. 5, 1986, pp 303–305.

16 D. He, and D. R. Hall, "Frequency Dependence in RF Discharge Excited Waveguide CO_2 Lasers," *IEEE J. of Quant. Electron*, Vol. 20, no. 5, 1984, pp 509–514.

17 F. Moghbeli, D. He, G. Allcock, and D. R. Hall, "Impedance matching in radio–frequency discharge excited lasers," *J. Phys E: Sci. Instrum.*, Vol. 17, 1984, pp 1159–1164.

18 G. Allcock, and D. R. Hall, "An Efficient, RF Excited, Waveguide CO_2 Laser," *Optics Comm.*, Vol. 37, no. 1, 1981, pp 49–52.

19 E. Garmire, T. McMahon, and M. Bass, "Flexible Infrared Waveguides for High Power Transmission," *IEEE J. of Quant. Electron.*, vol. QE-16, no.1, pp. 23-32, 1980.

20 M. J. Adams, *An Introduction to Optical Waveguides*, John Wiley and Sons, New York, pp 199-200, 1981.

21 K. D. Laakmann, and W. H. Steir, "Waveguides: Characteristic Modes of Hollow Rectangular Dielectric Waveguides," *Appl. Opt.*, Vol. 15, no. 5, May 1976, pp 1334-1340.

22 E. Garmire, T. McMahon, and M. Bass, "Flexible Infrared-transmissive Metal Waveguides," *Appl. Phys. Lett.*, Vol. 29, no. 4, Aug 1976, pp 254-256.

23 C. A. Hill, and D. R. Hall, "Waveguide Laser Resonators with a Tilted Mirror," *IEEE J. of Quant. Electron.*, Vol. QE-22, no. 7, July 1986, pp 11078-1087.

24 P. Mazur, and D. L. Mills, "Surface Roughness and the Attenuarion Length of Guided Waves in Optical Fibers," *J. Appl. Phys.*, Vol. 54, no. 7, 1983, pp 3735-3742.

25 U. Kubo, and Y. Hashishin, "Hollow light guide tube for CO_2 laser beam," *SPIE*, Vol. 713, Optical Fibers in Medicine, 1986, pp 17-21.

26 Traditionally, CO_2 surgical lasers have been delivered to the operating field by articulated mirror guides with limited circular entrance apertures.

27 O. L. Bourne and P. Dyer, "A Novel Stable–Unstable Resonator for Beam Control of Rare–Gas Halide Laser," *Optics Comm.*, Vol. 31, no. 2, 1979, pp 193-196.

28 A. E. Siegman, *Lasers*, University Science Books, Mill Valley Calif., U.S.A., 1986.

29 A. E. Siegman, "Unstable Optical Resonators for Laser Applications," *Proc. IEEE*, Vol. 53, 1965, pp 277-287.

30 R. J. Freiberg, P. P. Chenausky, and C. J. Buczek, "An Experimental Study of Unstable Confocal CO_2 Resonators," *IEEE J. of Quant. Electron*, Vol. QE–8, no. 12, 1972, pp 882-892.

31 S. L. Prunty, "A Compact Formula For The Coupling Efficiency Associated With Mirrors In Waveguide Lasers," *Int. J. of Infrared and Mill. Waves*, Vol. 6, no. 6, 1985, pp 471-479.

32 G. W. Sutton, M. M. Weiner, and S. A. Mani, "Fraunhofer Diffraction Patterns From Uniformly Illuminated Square Output Apertures With Noncentered Square Obscurations," *Appl. Opt.*, Vol. 15, no. 9, 1976, pp 2228-2232.

33 D. He, and D. R. Hall,"Frequency Dependence in RF discharge Excited Waveguide CO_2 Lasers," *IEEE J. of Quant. Electron*, Vol. QE–20, no. 5, 1984, pp 509-514.

34 D. He, D. R. Hall, "Longitudinal Voltage Distribution in Transverse RF Discharge Waveguide Lasers," *J. Appl. Phys.*, Vol. 54, no. 8, 1983, pp 4367-4373.

35 P. Lavigne, G. Otis, and D. Vincent, "Performance Characteristics Of A CO_2 Waveguide Laser," DREV R-4150/79, 1979.

36 W. W. Rigrod, "Saturation Effects in High–Gain Lasers," *J. Appl. Phys.*, Vol. 36, no. 8, 1965, pp 2487-2490.

37 A 20 cm long slab discharge laser has been constructed in the Medical Laser Lab with a reported output of better than 75 watts. Personal communication with M. D. Paulson.

38 L. Levi, *Applied Optics*, John Wiley and Sons, Inc., New York, 1968.

39 J.J. Degan, and D. R. Hall, "Finite–Aperture Waveguide–Laser Resonators," *IEEE J. of Quant. Electron*, Vol. QE–9, no. 9, 1973, pp 901–910.

40 R. L. Abrams, and W. B. Bridges, "Characteristics of Sealed–off Waveguide CO_2 Lasers," *IEEE J. of Quant. Electron*, Vol. QE–9, no. 9, 1973, pp 940–946.

41 F. Rosebury,*Handbook of Electron Tube and Vacuum Techniques*, Reinhold Publishing Corp., Ney York, 1967.

42 K. M. Abramski, A. D. Colley, H. J. Baker, and D. R. Hall, "Power Scaling of Large Area Transverse Radio Frequency Discharge CO_2 Lasers," Preprint submitted to *App. Phys. Lett.*, Nov. 1988.

43 G. A. Griffith, "Transverse RF Plasma Discharge Characterization for CO_2 Waveguide Lasers," *SPIE*, Vol. 227, 1980, pp 6–11.

44 The microsurface lathe located in the Department of Electrical Engineering, at the University of Alberta.

45 J. T. Verdeyen, *Laser Electronics*, Prentice–Hall, Inc., Englewood Cliffs, New Jersey, 1981.

46 A. K. Nath, H. J. J. Seguin, and V. A. Seguin, "Optimization Studies of a Multikilowatt PIE CO_2 Laser," *IEEE J. of Quant. Electron*, Vol. QE-22, no. 2, 1986, pp 286.

47 D. B. Rensch and A. N. Chester, "Iterative Diffraction Calculations of Transverse Mode Distributions in Confocal Unstable Laser Resonators," *Appl. Opt.*, Vol. 12, no. 5, 1973, pp 997-1010.